



COBALT TELETHERAPY SMALL FIELD DOSIMETRY

Lazola Jethro Nobecu

A research report submitted to the Faculty of Science, University of the Witwatersrand, Johannesburg, in partial fulfilment of the requirements for the degree of Master of Science in the field of Medical Physics.

2017

Declaration

I declare that the research report hereby submitted to the University of the Witwatersrand, for the degree of Master of Science in the field of Medical Physics has not previously been submitted by me for a degree at this or any other university; this is my work in design and in execution, and that all material contained herein has been duly acknowledged.

The University of the Witwatersrand Human Research Ethics Committee granted a waiver of ethics clearance (W-CJ-151204-1) for this work on the 4th December 2015.

L.J. Nobecu (Mr)

Dedications

To

My father Welile Jonas Nobecu, my mother Nokhaya Nobecu, my sisters, brothers and my friends, I would not have achieved this milestone if it was not for your love and support.

OOJAMBASE, OOHLATHI, OOLISA, AMAMFENE!!!

To my daughter, Amahle Phetogo Nobecu

Your kindness, sensitivity, and concern for others make us proud to be your Mom and Dad.

Pulane and I love you very much.

Acknowledgements and thanks

My special thanks to Professor Debbie Van der Merwe for giving me an opportunity to be part of this work. Thank you Prof. D for your massive input, guidance, patience and the suggestions you have made to this work. I would like to thank Mr. Nkosi Maphumulo for assisting me with the operation of the equipment, guidance and your experience that you selflessly shared with me. I also want to thank the Charlotte Maxeke Johannesburg Academic Hospital for allowing me to use their facility. A big thank you to the National Research Fund (NRF) and TATA Africa Scholarship for their appreciated assistance in funding my studies.

Table of Contents

Declaration.....	i
Dedications.....	ii
Acknowledgements and thanks.....	iii
Table of Contents.....	iv
List of figures.....	1
List of tables.....	4
Abstract.....	5
Chapter 1. Introduction and Aims	7
1.1 History of Radiation therapy	8
1.1.1 ⁶⁰ Cobalt teletherapy unit	10
1.2 Detectors.....	11
1.2.1 Introduction	11
1.2.2 What are detectors?	11
1.2.3 Types of detectors	12
1.2.3.1 Ionisation chamber	12
1.2.4 Detector requirements	13
i. Stability.....	13
ii. Energy response	14
iii. Spatial resolution.....	14
iv. Dose Linearity	14
v. Perturbation.....	15
vi. Angular response	17
Chapter 2. Literature Review.....	18
2.1 Detectors.....	20
2.2 Advantages and disadvantages of different detector types for small field dosimetry....	21

Chapter 3. The challenges of small photon fields	22
3.1 Definition of Output Factors	22
3.2 Partial Occlusion of the direct beam source	24
3.3 Charge Particle Equilibrium.....	27
3.4 Lateral Electronic Equilibrium.....	28
3.5 Polarity effect	29
3.6 Ion recombination and Collection efficiency	30
3.7 Determination of the small field equivalent square	31
Chapter 4. Materials and Methodology	32
4.1 Types and Properties of Radiation Detectors used.....	32
4.1.1 Ionization Chambers: PTW-31006 pinpoint 0.015 cm ³	32
4.1.2 PTW-31016 3D pinpoint 0.016 cm ³	33
4.1.3 PTW-31010 semiflex 0.125 cm ³	33
4.1.4 PTW-M30013 Farmer 0.6 cm ³	34
4.2 Methodology	34
Chapter 5. Results analysis and Discussion.....	37
5.1: Dose profiles	37
5.2 Comparison of the Dose Beam Profiles measurements of all detectors	41
5.3 Cross calibration.....	44
5.4 Daisy Chain method	46
5.5 Relative Output Factors.....	46
5.5.1: Comparison of Relative Output Factor Measurements from all Detectors.....	46
5.7: Uncertainty Budget	48
Chapter 6. Conclusions.....	50
Chapter 7. References.....	51

List of figures

Figure 1.1: MDS Nordion Equinox, (S/N 2009) ⁶⁰ Cobalt teletherapy unit at Charlotte Maxeke Johannesburg Academic Hospital.....	9
Figure 1.2: The schematic drawing showing the head of a ⁶⁰ Cobalt unit. Note where the source is kept when the beam is off and how it is shielded for safety.....	10
Figure 1.3: Schematic representation of a dosimeter as a sensitive volume (V) containing medium (g), surrounded by a wall of medium (w) and thickness (t).....	12
Figure 1.4: A diagrammatic representation of perturbation correction factors as they are applied to ionisation chambers in small fields. The central electrode effect is investigated by removing the electrode. Wall effect is removed by changing the wall to water and the air volume is replaced by water. Lastly, the volume averaging over the large water volume is compared to a 1 mm ³ voxel.....	16
Figure 2.1: Flow chart diagram describing the absolute dose calibration concept.....	19
Figure 2.2: A thimble chamber having a central electrode (anode) and a cylindrical chamber wall (cathode). A guard on central electrode potential limiting stem effect and dark current. An electrometer is connected.....	20
Figure 3.1: Positioning of a detector for the determination of output factors in a water tank at a fixed depth for reference field size and small field size.....	22
Figure 3.2: An example of the difference in the output factors obtained when using a Diode, Semiflex 0.125 cc ionization chamber, a diamond detector, a Pinpoint 0.015 cm ³ ionization and a microLion ionization chambers in a 6 MV beam.....	23
Figure 3.3: The geometric penumbra, which results from the size of the source diameter, may be reduced by employing a source capsule with 1.5 cm or less, the penumbra width increases with increase in source diameter, SSD, and depth but decreases with an increase in SDD. The geometric penumbra, however, is independent of field size as long as the movement of the diaphragm is in one plane, that is, SDD stays constant with increase in field size.....	25

Figure 3.4: The properties of a conventional field. The radiation source is clearly visible at the point of measurement, where the detector is positioned. The dose at the centre of the field is uniform.....26

Figure 3.5: Properties of a small field. When the field size is minimised to small field size, the small opening of collimators blocks the extended radiation source partially. The dose at the centre of the small field is non-uniform.....27

Figure 3.6: The concept of the charged particle equilibrium (CPE). When CPE exists, each charged particle (e_1) carrying energy E out of volume with the gas (cavity), the energy lost is compensated by another charged particle (e_2) carrying the same amount of energy into the volume.....28

Figure 3.7: The loss of lateral electronic equilibrium (LEE) close to the edge of a high energy photon represented by the dotted lines.....29

Figure 4.1: Ultra small-sized pinpoint therapy chamber for dosimetry in high-energy photon beams.....32

Figure 4.2: Ultra small-sized pinpoint therapy chamber with 3 dimensional characteristics for dosimetry in high-energy photon beams.....33

Figure 4.3: Standard therapy chamber for scanning systems and for absolute dosimetry.....33

Figure 4.4: Waterproof therapy chamber for absolute dosimetry in high-energy photon, electron and proton beams.....34

Figure 4.5: The two types of PTW ionization chambers and the PTW MP3 water phantom used to determine the OFs, A: PTW 31016 3D chamber positioned parallel to the central axis of the beam, B: PTW 31010 semiflex chamber positioned perpendicular to the central axis of the beam.....36

Figure 4.6: A PTW Unidos electrometer that was used to measure the charge, a Lufft Opus 20 temperature, humidity, air pressure data logger device for determining the pressure and the temperature in the room, and the mercury thermometer that was used for measuring the water temperature in the water tank. All these devices were used for measurements during the experiment.....36

Figure 5.1: In plane (blue lines) and cross plane (red lines) profiles at a depth of 10 cm for field sizes of 10 cm × 10 cm, 6 cm × 6 cm, 4 cm × 4 cm, 3 cm × 3 cm, 2 cm × 2 cm and 1 cm × 1 cm in a ⁶⁰Cobalt beam using a PTW 31016 3D ionization chamber, positioned parallel to the central axis of the beam at SAD = 80 cm. The profiles are normalised to the dose at the central axis for each field size.....37

Figure 5.2: In plane (blue lines) and cross plane (red lines) profiles at a depth of 10 cm for field sizes of 10 cm × 10 cm, 6 cm × 6 cm, 4 cm × 4 cm, 3 cm × 3 cm and 2 cm × 2 cm in a ⁶⁰Cobalt beam using a PTW 31006 ionization chamber, positioned perpendicular to the central axis of the beam at SAD = 80 cm. The profiles are normalised to the dose at the central axis for each field size.....38

Figure 5.3: In plane (blue lines) and cross plane (red lines) profiles at a depth of 10 cm for field sizes of 10 cm × 10 cm, 6 cm × 6 cm, 4 cm × 4 cm, 3 cm × 3 cm and 2 cm × 2 cm in a ⁶⁰Cobalt beam using a PTW 31010 ionization chamber, positioned perpendicular to the central axis of the beam at SAD = 80 cm. The profiles are normalised to the dose at the central axis for each field size.....39

Figure 5.4.: The dose profiles taken in a water tank from a ⁶⁰Cobalt photon beam. The field size was set at 10 cm × 10 cm, at depth of 10 cm and 80 cm SAD was used. The ionization chambers used were: PTW 31016 (Blue), PTW 31006 (Red) and PTW 31010 (Green).....41

Figure 5.6: The dose profiles taken in a water tank from a ⁶⁰Cobalt photon beam. The field size was set at 4 cm × 4 cm, at depth of 10 cm and 80 cm SAD. The ionization chambers used were: PTW 31016 (Blue), PTW 31006 (Red) and PTW 31010 (Green).....42

Figure 5.7: The dose profiles taken in a water tank from a ⁶⁰Cobalt photon beam. The field size was set at 2 cm × 2 cm, at depth of 10 cm and 80cm SAD. The ionization chambers used were: PTW 31016 (Blue), PTW 31006 (Red) and PTW 31010 (Green).....43

Figure 5.8: The dose profiles taken in a water tank from a ⁶⁰Cobalt photon beam. The field size was set at 1 cm × 1 cm, at depth of 10 cm and 80cm SAD. The ionization chambers used were: PTW 31016 (Blue), and PTW 31006 (Red).....46

Figure 5.9: Comparison of the relative output factors from the PTW 31006 pinpoint, PTW 31016 3D pinpoint and PTW 31010 semiflex with the BJR supplement 25 ⁶⁰Cobalt published data as a function of field size. The data are normalized to the field size of 10 cm × 10 cm. Error bars are shown for the measured data series and represent the percentage error with 5% value.....47

List of tables

Table 1: Calculations of the equivalent square fields for the field sizes of 10 cm × 10 cm, 6 cm × 6 cm, 4 cm × 4 cm, 3 cm × 3 cm, 2 cm × 2 cm, 1 cm × 1 cm using the square fields determined by the chamber during the scanning, the ionization chambers were PTW 31010, PTW 31006 and PTW 31016 3D respectively.....40

Table 2: Cross calibration results of the small field chambers at 6 cm × 6 cm field size calibrated against the PTW 0.6 cm³ Farmer chamber with their uncertainties.....45

Table 3: Dose rate data obtained from the daisy chain measurements on 02/08/2016 in a field of 4 cm × 4 cm using PTW 30013 0.60 cm³ Farmer, PTW 31016 3D pinpoint 0.016 cm³, PTW 31006 pinpoint 0.015 cm³ and PTW 31010 semiflex 0.125 cm³ chambers. The measurements were performed at the depth of 10 cm, SAD of 80 cm in a water phantom. ...46

Table 4: Uncertainty budget with the type A and type B uncertainties. The percentage difference was 1.13% between the independent setups for which the OF were calculated, this uncertainty percentage is less as compared to small field dosimetry when using conventional ionization chambers.49

Abstract

Aim

The aim of this research was to contribute to clinical implementation of the small field dosimetry Code of Practice (CoP) that is due to be published by the International Atomic Energy Agency (IAEA) in collaboration with the American Association of Physicists in Medicine (AAPM) (1). A 6 cm × 6 cm virtual machine-specific reference (fmsr) field was established in a clinical ⁶⁰Cobalt teletherapy beam used for conventional radiotherapy at Charlotte Maxeke Johannesburg Academic Hospital, and relative output factors were measured down to a set field size of 1 cm × 1 cm using three different models of Physikalisch-Technische Werkstätten (PTW) small field ionization chambers.

Materials and Methodology

The measurements were all performed on a Cobalt teletherapy unit (MDS Nordion Equinox, S/N 2009) in a PTW MP3 water phantom. The small field ionization chambers that were used were a PTW 31016 3D pinpoint 0.016 cm³, a PTW 31006 pinpoint 0.015 cm³ and a PTW 31010 semiflex 0.125 cm³. A calibrated PTW 30013 Farmer 0.6 cm³ ionization chamber was used to provide traceability for the cross calibration. A “daisy chain” methodology was used to perform the cross calibration in a virtual fmsr field of 6 cm × 6 cm and then establish the absolute dose rate in a 4 cm × 4 cm field. Relative output factors as a function of field size were measured with each small field ionization chamber and then compared to published results.

Results

Small square fields from a ⁶⁰Cobalt beam were created using the secondary collimators integrated into the unit. Equivalent square fields were calculated using the profiles obtained by the three ionization chambers during scanning and were in agreement with the ones that were programmed into the console. The coincidence of the central axis of the beam and the point of measurement for each detector was determined from the beam profiles. The cross calibration and daisy chain measurements resulted in a consistent dose rate of within ± 0.6% in the 4 cm × 4 cm field when measured with the four different ionization chambers. For 6 cm × 6 cm, 4 cm × 4 cm, 3 cm × 3 cm and 2 cm × 2 cm field sizes, relative output factors obtained from the uncorrected detectors' response agreed to within ± 0.8 % between the three small field ionization chambers. The variation in the 1 cm × 1 cm field size was ± 8.1 %.

When compared to published data, large differences in field size correction factors were obtained.

Conclusion

Small field dosimetry in a $^{60}\text{Cobalt}$ photon beam using three different PTW small field ionization chamber models was investigated. A cross calibration in a virtual msr field was done followed by a daisy chain process to determine the dose rate in a small field. Dose profiles and relative output factors were then measured and compared. The lack of lateral charge particle equilibrium and volume averaging effect was evident when using the PTW 31010 semiflex chamber in a $1\text{ cm} \times 1\text{ cm}$ field. The PTW 31006 pinpoint and 31016 3D pinpoint were in close agreement for field sizes down to $1\text{ cm} \times 1\text{ cm}$ with the 3D pinpoint performing as the best detector in this study. The optimal positioning of a detector should be determined from beam profile scans and not the engineering diagrams. The PTW 31016 3D pinpoint and PTW 31006 pinpoint are recommended for the determination of output factors in small field sizes. However, field output correction factors are required for both detectors in field sizes under $2\text{ cm} \times 2\text{ cm}$. Small field data published in the British Journal of Radiology (BJR) Supplement 25 (2) should not be used to benchmark dosimetry in modern $^{60}\text{Cobalt}$ teletherapy units.

Chapter 1. Introduction and Aims

The aim of this research was:

- To contribute to clinical implementation of the small field dosimetry Code of Practice (CoP) that is due to be published by the International Atomic Energy Agency (IAEA) in collaboration with the American Association of Physicists in Medicine (AAPM) (1).
- To establish a 6 cm × 6 cm virtual machine-specific reference field in a clinical ⁶⁰Cobalt teletherapy beam used for conventional radiotherapy at Charlotte Maxeke Johannesburg Academic Hospital (CMJAH) and then determine the dose rate in a 4 cm × 4 cm field.
- To measure and compare output factors down to a set field size of 1 cm × 1 cm using three different models of Physikalisch-Technische Werkstätten (PTW) small field ionization chambers.

Radiation therapy plays an important role in fighting cancer and other malignant diseases (3). Small radiation fields e.g. stereotactic radiosurgery and radiotherapy, have been used for many decades before the introduction of advanced technologies (4). Recently the number of modalities that use small radiation fields have increased. These modalities allow the delivery of high doses to small volumes (5).

Small radiation fields exhibit complex dosimetry (6). One of the challenges is the absence of an international CoP that is dedicated solely to small radiation fields. The IAEA in collaboration with the AAPM are currently developing a small field dosimetry CoP and this work forms part of a coordinated research project to test its implementation in the clinical setting (1).

Physics challenges in small field dosimetry that have been identified in many studies (5; 7; 8; 9) include:

- Lack of secondary electron equilibrium.
- Detector volume averaging effect.
- Perturbation of the photon fluence by a detector.
- Complex modelling of small field.

Small field detectors are being developed and tested continuously. These detectors are ideally physically small i.e. volume $< 0.0125 \text{ cm}^3$, not dependent on dose rate, have no directional influences and have improved spatial resolution (5; 10). In this research, three PTW different models detectors were used to determine the dose rate and output factors in a ^{60}Co teletherapy unit according to the methodology in the IAEA/AAPM CoP that is in press (1).

1.1 History of Radiation therapy

Cancer is a public health crisis throughout the world and is responsible for just over a quarter of all deaths. It exceeds mortality due to cardiac diseases, which in many countries, were the leading causes of death to people below the age of 85 in 2007 (11; 12). In 2020, An approximation of about 20 million new cases are expected internationally; these new cases will mostly affect the population in developing countries where there are more people and less financial resources (13). Prior to the introduction of ionizing uncharged and charged particle beams, the field of medicine had limited modalities for controlling and treating cancer. Radiation therapy advanced over four major stages. The first stage was the discovery of x-rays by Wilhelm Roentgen in 1895 followed by the discovery of radioactivity by Henri Becquerel (1896) and of radium by Marie Curie (1898) (14). Both x-rays and radium sources were quickly adopted for medical applications (14). X-rays were applied in radiation medicine in 1920 (11). The second stage was the introduction of kilovoltage x-ray therapy in the late 1920s and this continues to today.

The treatment of deep-seated tumors was limited by the maximum energy of the x-ray tube. In the 1920s, physics and engineering developments led to an in depth knowledge of subatomic particles and this contributed to an increase in the radiation energies available to medicine (15). The third stage was the development of megavoltage energies between the years 1946 – 1996. $^{60}\text{Cobalt}$ teletherapy was employed as a source of high energy gamma rays for external beam radiotherapy followed by linear accelerators (LINACs). $^{60}\text{Cobalt}$ produces gamma rays of 1.17 and 1.33 MeV. The 1.25 MeV average energy allows penetration of the beam to deeper tumors with skin sparing. The last stage refers to developments in techniques that are associated with advances in technology (11; 15). Figure 1.1 shows a $^{60}\text{Cobalt}$ teletherapy unit.



Figure 1.1: MDS Nordion Equinox, (S/N 2009) ^{60}Co teletherapy unit at Charlotte Maxeke Johannesburg Academic Hospital.

Charged particle therapy (CPT) or hadron therapy was mostly developed by nuclear and medical physicists (16). The idea of accelerating ions for therapeutic purposes arises from their useful depth dose distributions inside the tumor (17). In 1946, R Wilson who was a student at the University of California, proposed the therapeutic use of protons for treating deep seated cancer cells (16). Proton radiotherapy has become an advanced CPT and the therapy of heavier ions (i.e. ^{12}C Carbon) has become even more attractive. CPT allows a reduction of the dose delivered to organs at risk (OARs) as compared to photon therapy (17). The Bragg curve of charged particles makes these modalities able to deliver radiation dose to some tumors better than photons. CPT has also been successfully employed in small field treatments (18). The same challenges in small proton field therapy dosimetry exist as in small photon field dosimetry because CoPs only apply to reference dosimetry in conventional fields (18).

1.1.1 ⁶⁰Cobalt teletherapy unit

In a ⁶⁰Cobalt teletherapy unit, the radiation source is usually at a distance of 80 or 100 cm from the isocentre whereas in LINACs, the isocentre is 100 cm from the focal spot (19). The advantages of ⁶⁰Cobalt sources are its high energy of emitted photons, long half-life, high specific activity, and large specific air kerma rate constant (Γ_{AKR}) (20). ⁶⁰Cobalt teletherapy units have low operating costs (20), and decreased maintenance and downtime as compared with LINACs (21). ⁶⁰Cobalt is produced by bombarding ⁵⁹Cobalt with neutrons inside a reactor (22). Sources of very high specific activity amounting to 300 Ci/g and high source strength of about 10 kCi are used in teletherapy machines (23). Figure 1.2 shows a schematic diagram of a ⁶⁰Cobalt teletherapy unit head.

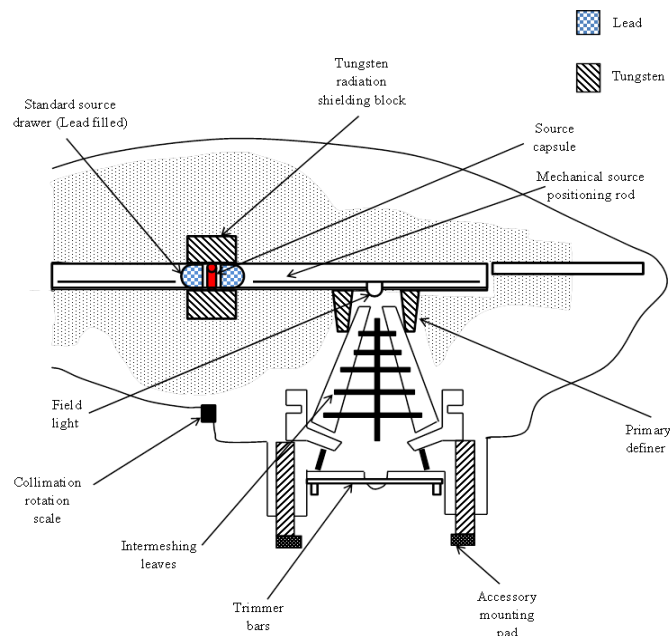


Figure 1.2: The schematic drawing showing the head of a ⁶⁰Cobalt unit. Note where the source is kept when the beam is off and how it is shielded for safety (24) .

Although LINACs offer different beam characteristics such as lower penumbra, higher energies and rapid treatments, they are more expensive, require a more sophisticated infrastructure and are highly complex. In low and middle-income countries and most African countries, ⁶⁰Cobalt teletherapy units may be more suitable than LINACs (25; 26; 27).

The simplicity of a ⁶⁰Cobalt teletherapy unit gives added advantages of less downtime, less maintenance and running costs when compared with LINACs. Another important advantage

of $^{60}\text{Cobalt}$ teletherapy units is the ability to use $^{60}\text{Cobalt}$ beam for conformal and intensity modulated radiotherapy (IMRT) which are considered to be advanced treatment techniques (28).

1.2 Detectors

1.2.1 Introduction

Modern radiation therapy requires the precise, secure and “reproducible delivery of complex three dimensional (3D) radiation dose distributions”. National and international requirements for medical radiation safety and traceable calibration must also be satisfied (29). Radiation detectors used in radiation therapy therefore play a very important supporting role in performing dosimetry measurements. A range of unique detector systems are utilised for different types of dosimetry measurements (30). The two major types of the measurements are:

- 1 Quality assurance of equipment, and
- 2 Verification of treatment delivery.

The main types of detectors fall into the following groups: detectors used to estimate point doses e.g. air ionization chambers, semiconductor detectors, thermoluminescent detectors (TLDs), etc. and detectors for planar dose e.g. radiographic film and electronic portal imagers. (31).

1.2.2 What are detectors?

A detector is a sensitive device that is capable of providing a reading (r) that is a measure of the absorbed dose (D_g) deposited in the device’s sensitive volume (V) by the ionizing radiation. If the dose is not distributed uniformly throughout the sensitive volume of the detector, then r is a measure of the average value of the dose (D_g) (32). Figure 1.3 shows a schematic representation of a detector.

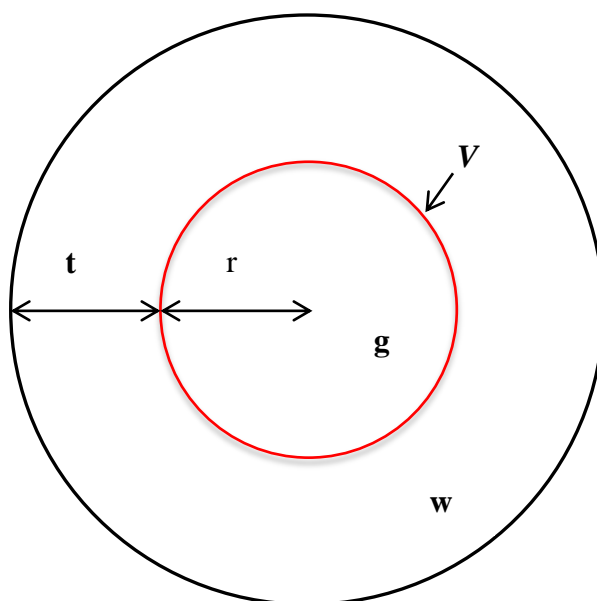


Figure 1.3: Schematic representation of a detector as a sensitive volume (V) containing medium (g), surrounded by a wall of medium (w) and thickness (t) (33).

Ideally, radius (r) is considered to be directly proportional to (D_g), and each volume element of (V) has equal influence on the value of (r) which means that (D_g) is in fact the mean dose throughout the volume (V). This principle is often but not always well approximated in practical detectors. A detector can be treated in terms of cavity theory. The sensitive volume (V) can be taken as the cavity which may contain gas, liquid or solid medium (g), depending on the type of a detector. Cavity theory gives one of the most useful means of interpretation of a detector reading (32; 33).

1.2.3 Types of detectors

1.2.3.1 Ionisation chamber

The absorbed dose in any medium cannot be measured easily, especially by direct methods. When dosimetry measurements are being performed using an ionization chamber, they are based upon replacing a small volume of the medium by an air cavity in which the ionization

of air by the radiation can be measured and to which the dose to the medium can be related. When a medium is uniformly irradiated by electrons, the fluence of electrons will be the same at all points within the medium. If a small air cavity of a certain size is used such that it does not bring about changes to the energy spectrum or the number of electrons in the cavity (i.e. does not perturb the electron fluence), then the fluence of electrons in the air is the same as it would be in the medium. The cavity is then termed a Bragg- Gray cavity (34).

The construction of an ionization chamber may introduce perturbations both to the fluence of electrons crossing the air cavity and to the photon beam itself. A wall of infinitesimally small thickness may be considered as having no impact on either, such that the chamber is effectively an air cavity within the medium. In small field dosimetry, in a case where the density of the sensitive volume of the detector is high, the detector will over respond and when low, the detector will under respond (35). As the wall increases in thickness, an increasing percentage of the secondary electrons crossing the air volume will be from the wall rather than the medium until, in the extreme, all electrons crossing the air volume originate from within the wall. In this situation, the electron fluence across the air volume is the same as the fluence within the wall, and the ionization can then only be related to the dose to the wall (36). The existence of extra-cameral components of high atomic number (Z) can result in an increase of the detector response when used in small field dosimetry (35).

1.2.4 Detector requirements

i. Stability

All the measurements of any parameter taken using a detector have an uncertainty that is a combination of the uncertainties related to the measuring device itself coupled with the uncertainties in the methodology that has been used in the measurement and the inconstancy of the actual parameter that is being measured. “The combined stability of the whole measurement system, adding the variations in the beam output is denoted by the standard deviation of measurements taken where all the controllable conditions of irradiation remain the same. Non-stabilities can lead to modifications in the detector response due to the irradiation history of the system, and a requirement is that the short term detector response

should be less than 0.1 percent for a total combined dose of many hundreds of kGy from numerous exposures (10). When recalibration is not performed frequently, the correction for non-stabilities over time can be made only if the effect of non-stabilities is consistent. Non-reversible degrading of the detector may lead to long term changes (7)".

ii. Energy response

Detectors that are used in small field sizes should have a useful energy range up to 30 MeV for photons (37). Mass energy absorption coefficients (μ^{en}/ρ) and collisional stopping power (S/ρ) data are available for most detector materials (air, silicon, and carbon). A perfect detector should be water equivalent and would not be affected by variations in (μ^{en}/ρ) and (S/ρ) from low energy photon contributions (20).

iii. Spatial resolution

The measurement device should offer good spatial resolution in at least one dimension. The need for spatial resolution is normally determined by the gradients in the quantity that is going to be measured. A suitable detector in terms of spatial resolution results in a trade-off between a high signal to noise ratio (SNR) and the size of the detector (7). This trade-off has a huge impact in the accuracy of the measurement, more especially in challenging conditions of steep dose gradients (30). When the size of the ionization chamber increases, the spatial resolution decreases (7).

iv. Dose Linearity

A dosimeter reading should be linearly proportional to the dose rate that is relevant to the techniques that will be employed (38). The signal of the detector (A) versus the dose rate (\dot{D}) can be represented by the following equation:

$$A = A_{dark} + R \cdot \dot{D}^\Delta \dots\dots\dots 1$$

When $\Delta = 1$, the relationship becomes linear. A_{dark} is the signal as a result of the dark current of the detector and R is the detector specific constant. The boundaries to the range are determined by the background reading (zero dose/noise) at the lower end and the possible over response of the detector until a final saturation of the signal has been achieved at high doses (39).

v. Perturbation

Perturbation of the electron fluence in the medium will always exist when there is a detector present in the irradiated medium (40). The size of the detector has a perturbing effect on the photon fluence unless the detector has ideal tissue equivalent properties. Perturbation that is caused by a detector is normally considered as a shift from Bragg-Gray Cavity theory. If the size of cavity is smaller than the range of the charged particles, this means that the cavity is not perturbing the photon fluence (41). When the size of the field decreases, charged particle equilibrium is no longer achieved and the conditions for cavity theory fail due to the changes in lateral scatter conditions. When a detector is positioned within a small field, it causes perturbation that is difficult to quantify because the major source of the effect is the disturbance of photon fluence. The use of large field replacement correction factors is not possible because the perturbation is highly dependent on the detector shape (42).

Perturbation factors in small field dosimetry are very important. Reference dosimetry is generally performed by using the absorbed dose to water calibration factor N_{D,wQ_0} obtained in a 10 cm × 10 cm reference field size using a reference beam (usually $Q_0 = {}^{60}\text{Cobalt}$ beam). The dose in reference conditions at a different beam quality Q is obtained by applying the beam quality correction factor (K_{Q,Q_0}).

When using the IAEA Technical Report Series Number 398 (IAEA TRS 398) CoP (43), ionization chambers are positioned with the centre at reference depth (z_{ref}) and the correction factor for perturbation (P_{dis}) is applied in k_{Q,Q_0} . This is because the ion chamber disturbs the electron fluence at a point closer to the radiation source than z_{ref} . In small field dosimetry, a different conversion is introduced for the determination of dose at the reference depth. Figure

1.4 shows that the central electrode influence is dealt with first by applying the electrode perturbation correction factor (P_{cel}). Secondly, the wall influence is removed by applying the wall perturbation factor changing the wall to water. Thirdly, the air volume is replaced by water. Finally, the volume averaging over the large water volume is compared with a small voxel (44).

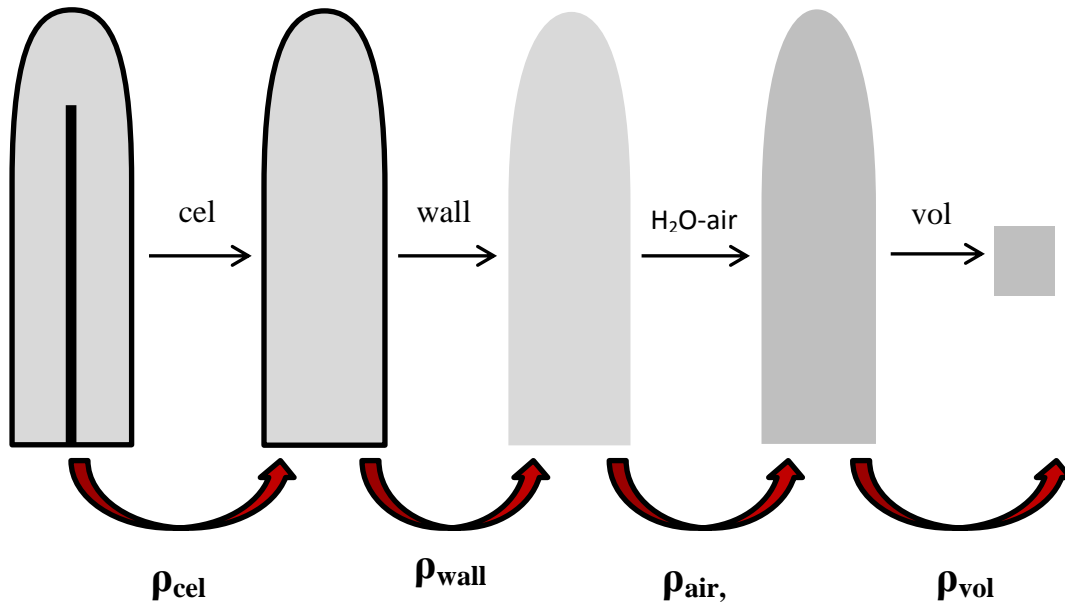


Figure 1.4: A diagrammatic representation of perturbation correction factors as they are applied to ionisation chambers in small fields. The central electrode effect is investigated by removing the electrode. Wall effect is removed by changing the wall to water and the air volume is replaced by water. Lastly, the volume averaging over the large water volume is compared to a 1 mm^3 voxel (44).

“The perturbation factors are therefore:

- The central electrode perturbation factor P_{cel} ,
- The wall perturbation factor P_{wall}
- The fact that the cavity is air-filled instead of water
- The volume averaging due to the relative large water volume. $P_{\text{vol,w}}$ is the perturbation for the relative large replacement water volume of the detector compared to a 1 mm^3 voxel” (45).

vi. Angular response

The response of a detector should not depend on the orientation of the detector with respect to the incident beam axis. The variation due to the detector orientation should not be more than $\pm 0.5\%$ for $\pm 60^\circ$ beam incidence relative to the axis of the detector (7). This makes precise detector positioning at the point of measurement a lot more important than when performing dosimetry in conventional fields. (5).

Chapter 2. Literature Review

An International CoP for Static Small Field Dosimetry is due to be published by the IAEA in collaboration with the AAPM (46). Current clinical absorbed dose to water CoPs such as the AAPM Task Group Number 51 (AAPM TG-51) (47) and the IAEA TRS-398 require dosimetry to be performed under reference conditions. In small photon fields, these conditions cannot be satisfied. To solve this problem, a new formalism for small photon and composite fields has been presented by IAEA and AAPM. It introduces the concept of two new intermediate calibration fields, which will be used in small field dosimetry (46).

A number of dosimeters and detectors have been developed for small field dosimetry which improve on the spatial resolution, perturbation effects, volumetric effects and/or sensitivity as compared to the dosimeters and detectors that are employed for conventional dosimetry of high energy photon beams (46). The new CoP advises a range of detectors that are more suitable to perform these dosimetric measurements in small field beams (3;52;).

A rising number of external beam treatment methods make use of very small radiation fields. On the other hand, stereotactic radiosurgery (SRS) has been used for many years. Newer approaches include Stereotactic body radiotherapy (SBRT), intensity modulated radiation therapy (IMRT) and volumetric arc therapy (VMAT) (5). Alfonso, et al. (46) pointed out that in small fields, clinical dosimetry has more uncertainty than in conventional beams. Aspraddakis, et al (48) showed that serious dosimetric errors have negatively affected many patients when small fields were employed in the delivery of high radiation doses. Dosimetric errors were often caused by reference conditions that were recommended by classical CoPs which were not established in some treatment units (49).

As highlighted by Wuerfel (5), small field dosimetry invalidates Bragg Gray cavity theory conditions of traditional dosimetry. Two types of intermediate calibration conditions were then suggested, one being the machine-specific reference field (fmsr) and the other the plan-class specific reference field (pcsr). For fmsr, Alfonso et al (46) assumes that a reference field condition can be delivered by a static beam at the user's facility. It was designed to address the calibration needs of stereotactic radiosurgery but can also be used for IMRT systems that cannot deliver the standard 10 cm × 10 cm reference field. For fmsr fields three approaches are recommended in order of preference:

- The use of an ionization chamber calibrated specifically for the fmsr field,
- the use of an ionization chamber calibrated in a conventional reference field with a generic correction factor for the fmsr field,
- the use of an ionization chamber calibrated in a conventional reference field with the product of a correction factor for a virtual reference field and a correction factor for the difference between the fmsr and virtual fields (46; 50; 51).

Dieterich et al (52) defines the pcsr field as the field that can be used in conjunction with an fmsr calibration or as a stand-alone. The pcsr field consists of a combination of multiple fields, which is close to a clinical class of patient plans (e.g. prostate plan). Pcsr fields should deliver a homogenous dose to an extended volume such that the dose can be measured without incurring errors from perturbation and volume averaging effects. The advantage of using the pcsr field method is the overlay of individual beams that compensates for the lack of dose homogeneity and electron equilibrium in large penumbral regions of small fields.

Alfonso et al (46) and Dieterich et al (52) add that for any clinical radiation teletherapy unit used with small fields, a standard reference dose calibration using CoPs such as IAEA TRS-398 or AAPM TG-51 should be used, if it is available. If a 10 cm × 10 cm square field is unavailable, (fmsr) and (pcsr) fields should be used. Figure 2.1 demonstrates the concept proposed as a flow chart diagram.

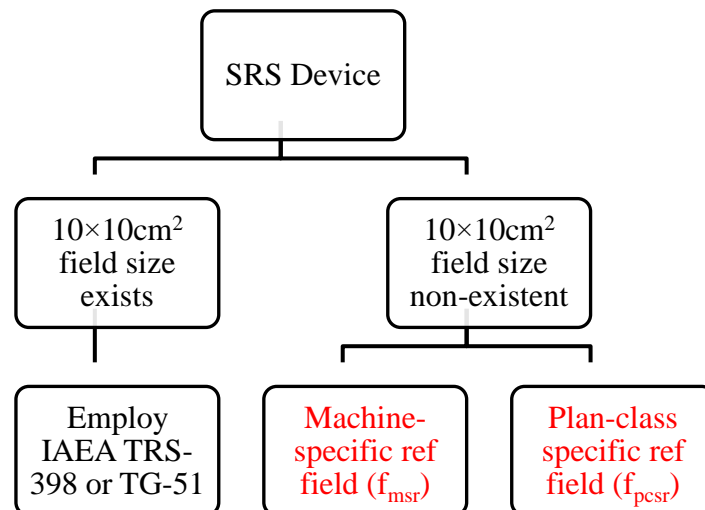


Figure 2.1: Flow chart diagram of the concept proposed describing the absolute dose calibration concept for small field sizes (8).

2.1 Detectors

Accurate dosimetric characterization of clinical radiation beams is crucial for accurate dosimetry. The accuracy requirement is compounded when dose is delivered through multiple small field beamlets (34).

Different detectors have different properties and advantages when used in small field measurements. The ionization chamber is the most widely used detector for accurate absolute dosimetry (53). An ionization chamber has a gas volume that is found between the two electrodes: anode and cathode. These electrodes are connected to high voltages of 100 V to 1000 V. When this gas volume is irradiated, positive charge carriers and negative charge carriers are created. The positive charge carriers are attracted to the cathode electrode and the negative charge carriers are attracted to the anode electrode thus creating a current which is measured by the use of an electrometer (54). Figure 2.2 shows a schematic diagram of a thimble chamber.

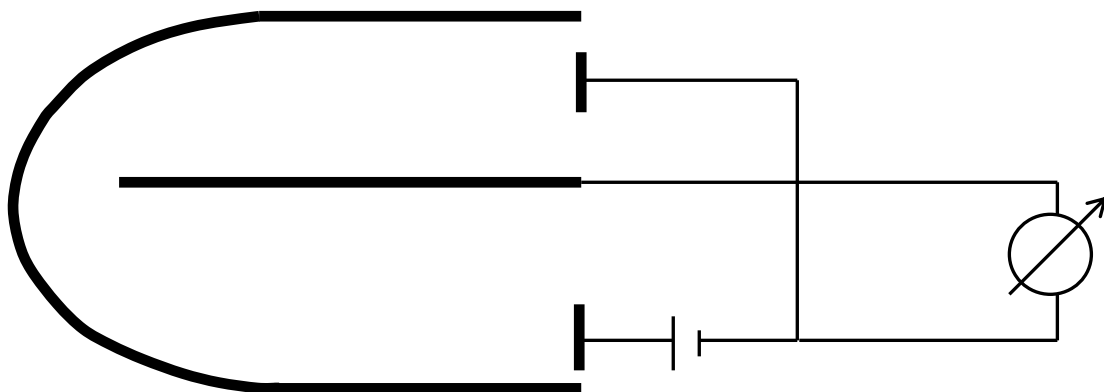


Figure 2.2: A thimble chamber having a central electrode (anode) and a cylindrical chamber wall (cathode). A guard on the central electrode potential limits the stem effect and dark current. An electrometer is connected (54).

2.2 Advantages and disadvantages of different detector types for small field dosimetry.

Diode detectors feature the highest response per volume of all common detector types. The size of their sensitive volume is usually small enough to avoid dose volume effects down to very small fields. However, their directional response and their response to low energy scattered photons is sometimes not ideal. To reduce the effect of low energy photons, silicon diodes are available in a shielded design where the shield reduces the signal from these photons for instance. In small fields the low energy scatter contribution is low, hence diode shielding is not needed and unshielded diodes are also recommended for small fields (34).

Medium-size vented ionization chambers have a sensitive volume between 0.1 cm³ and 1.0 cm³. Their only disadvantage is the relatively large size which can lead to a larger volume averaging effect. They are ideal for small field dosimetry down to field sizes of 3 cm × 3 cm, depending on the model in question. Small-size air filled vented ionization chambers (Pinpoint chambers) have a sensitive volume of the order of 0.01 cm³. They can typically be used for dose measurements in fields down to 2 cm × 2 cm. Care must be taken if pinpoint chambers are used in very large fields where stem and cable effects become important. Ionization chambers with steel electrodes demonstrate stronger energy dependence (5). Li et al (55) explains that an ionization chamber with build-up caps made of aluminium, copper, lead or Polytetrafluoroethylene (PTFE) are used in order to measure small fields, achieve electron equilibrium and to achieve sufficient effective depth of the measuring point to measure beyond the range of contaminant electrons.

Scott et al (56) compared spherical pinpoint chambers and how they influence perturbation factors. The PTW 31016 3D had smaller perturbation factors than other pinpoint ionization chambers such as PTW 31006, PTW 31014, and PTW 31015. In addition, Scott et al (56) determined large polarity effects in small field sizes when pinpoint chambers were used. Swanpalmer et al (57) highlighted that the cylindrical ionization chamber radius of the air cavity plays a role in influencing the mass ionization in the depths of 5 cm and 10 cm. This concludes that normalization of the depth ionization curves at depth of maximum for cylindrical chambers with air cavity radii is not valid. Pisature et al (58) added that phantoms with low densities lead to higher perturbation effects as the difference in the range of secondary charged particles between the medium and the ionization chamber increases.

Chapter 3. The challenges of small photon fields

3.1 Definition of Output Factors

Output factors are utilized to characterize changes in dose rate as the field size changes. The relative output factor (OF) is defined as the ratio of the dose in (D_w) for a certain field size (F) at a reference depth (d) to the dose at the same point and depth for the reference field size (F_{ref}). OF can be calculated using equation 7 below:

$$OF = \frac{D_w(F,d)}{D_w(F_{ref},d)} \dots\dots\dots 7$$

In most cases the reference field is normally set to be 10 cm × 10 cm. For the reference field, the OF = 1 at any given depth. Field sizes that are greater than the reference field (> 10 cm × 10 cm), OF > 1, but for the field sizes less than the reference field as in the case of this report, OF < 1 (34). The setup for determining the relative output factors measurements is shown in Figure 3.1.

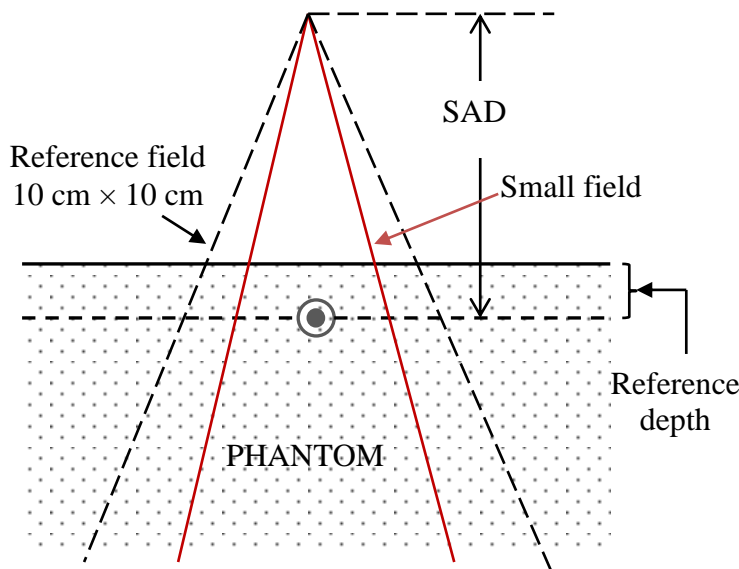


Figure 3.1: Positioning of a detector for the determination of relative output factors in a water tank at a fixed depth for reference field size and small field size (61).

As the field size changes, spectral changes in standard linear accelerators and cobalt units can occur due to differences in the exposure of the flattening filter (in case of LINACs) and scatter from the collimators. In small fields, the photon fluence across the field is not uniform. It has two or more overlapping penumbra regions (59). This leads to a beam profile with no area of uniform dose in which to position the detector which is in contrast to a larger reference field (6 cm × 6 cm or 10 cm × 10 cm). These conditions can assist in defining an ideal detector as one that has a uniform spectral response and a high SNR while being considered “small” enough (7). All detector signals average the response over the volume. A large detector will average the dose resulting from a signal in the centre of its volume that is different from a signal from a very small detector (5). This is known as the averaging effect (Volume Effect). The consequence of the averaging effect is that the dose at the field center is underestimated and the width of the penumbra measured from a beam profile appears wider than it really is (53).

Output factors of high-energy x-ray machines characterize the relative variation in dose with the size of the field normalised to a reference field size at a given depth in a phantom. Output factor is therefore a combination of collimator scatter factor, head-scatter factor and phantom-scatter factor (53; 55). Measurements of output factors in small fields with different detectors has resulted in discrepancies of the order to 20% (53) as shown in Figure 3.2.

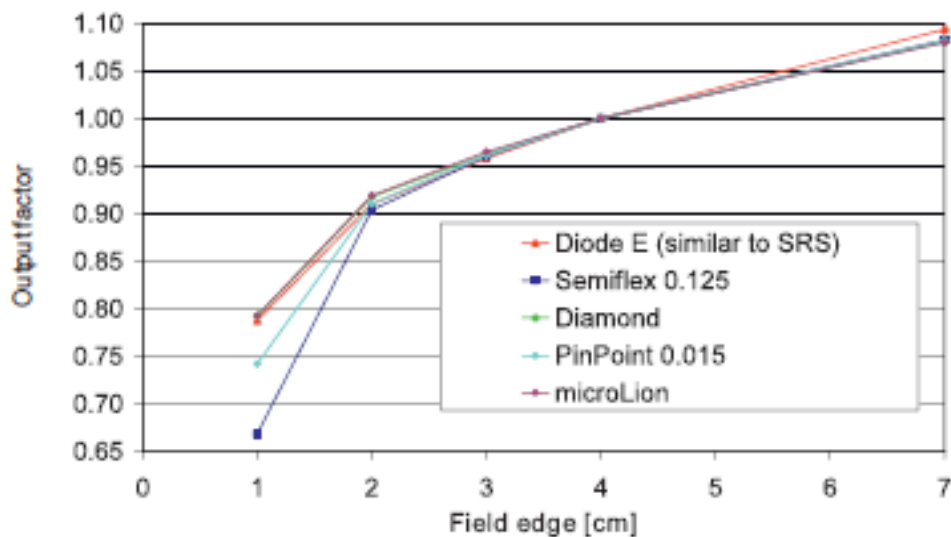


Figure 3.2: An example of the difference in the output factors obtained when using a Diode, Semiflex 0.125 cm³ ionization chamber, a diamond detector, a Pinpoint 0.015 cm³ ionization and a microLion ionization chamber in a 6 MV beam (53).

3.2 Partial Occlusion of the direct beam source

The term penumbra in general terms means, the region at the edge of a radiation beam, over which the dose rate changes rapidly as a function of distance from the beam axis. The penumbra width in a beam profile is described as the distance between the 80% and 20% isodose levels (10). The profile is made up of three components: the primary beam, geometric penumbra and the dosimetric penumbra. In a ⁶⁰Cobalt unit the high geometric penumbra is the result of the radiation source not being a point source (60). In small fields, the penumbra narrows increasingly as the collimator settings are reduced leading to the entire field being considered to be penumbra (7).

A collimator structure is made to adjust the size and shape of the beam in order to meet the requirements of different treatment techniques (61). The continuously adjustable diaphragm consists of two pairs of heavy metal blocks (X and Y jaws). Two forms the upper and the other two forms the lower jaws of the collimator system. Each pair can be operated independently to obtain a square or a rectangle shaped field at the isocentre of the machine (20). When the inner surface of the blocks is made parallel to the central axis of the beam, the radiation will pass through the edges of the collimating blocks resulting in what is known as transmission penumbra. Transmission penumbra cannot be removed completely but can be reduced by shaping the collimation blocks such that the inner surface is always parallel to the edge of the beam. The second type of penumbra is known as the geometric penumbra and is illustrated in figure. The geometric width of the penumbra (P_d) at any depth (d) from the surface of a patient can be determined by using similar triangles ABC and DEC (61).

From Figure 3.3 we have:

$$\frac{DE}{AB} = \frac{CE}{CA} = \frac{CD}{CB} = \frac{MN}{OM} = \frac{OF+FN-OM}{OM} \dots\dots\dots 5$$

If $AB = s$, the source diameter, $OM = SDD$, the source to diaphragm distance, $OF = SSD$, the source to surface distance, then from equation 5, the penumbra DE at depth (d) is given by:

$$P_d = \frac{s(SSD+d-SDD)}{SDD} \dots\dots\dots 6$$

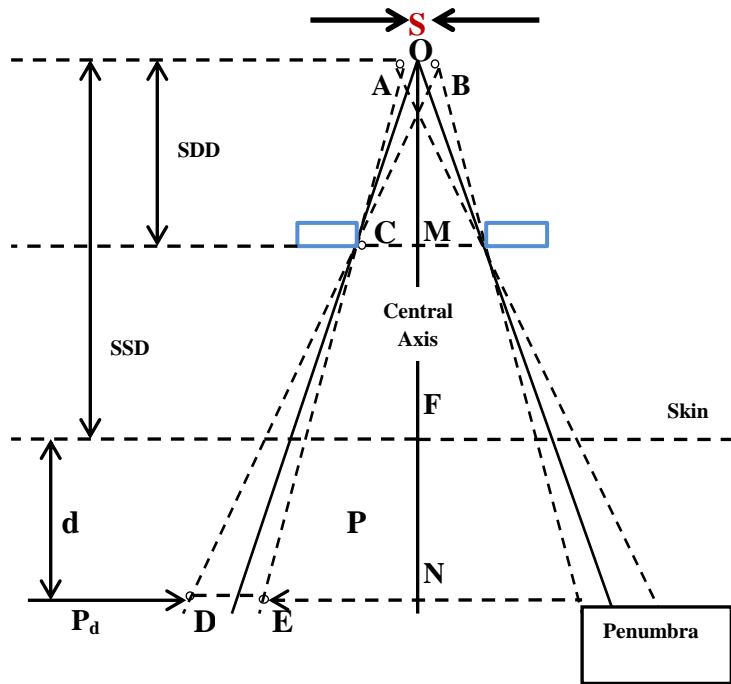


Figure 3.3: The geometric penumbra (which results from the source diameter) may be reduced by employing a source capsule with 1.5 cm or less. The penumbra width increases with an increase in source diameter, SSD and depth but decreases with an increase in SDD. The geometric penumbra however, is independent of field size as long as the movement of the diaphragm is in one plane, that is, the SDD stays constant with increase in field size (61).

The penumbra at the surface can be calculated by substituting $d = 0$ in equation 6. Equation 6 shows that the penumbra width increases with increase in source diameter, SSD, and depth but decreases with an increase in SDD (61). The geometric penumbra is independent of field size as long as the movement of the diaphragm is in one plane, that is, SDD stays constant with increase in field size (62). “With SDD as a vital parameter in determining the penumbra width, penumbra trimmers can increase SDD reducing penumbra width. Penumbra trimmers consists of heavy metal bars to absorb or scatter (attenuation) the beam in the penumbra region making beam edges to be sharp. The last penumbra is known as the physical penumbra. Physical penumbra width can be defined as the lateral distance between two specified isodose curves at a specific depth (62)”.

Photon fluence that is generated by either a Cobalt unit or an electron linear accelerator consists of a direct beam of radiation originating from a radiation source or at the target level

(focal spot) respectively. Indirect beam radiation (extra-focal spot radiation) occurs as a result of photons that have been scattered by the machine elements situated below the target. These elements include the primary collimator, flattening filter (LINACs), monitor chamber (LINACs) and the secondary collimator. Figure 3.4 shows how extra-focal radiation can contribute up to 8% of the beam output for a 6 MV beam (63). The focal spot radiation can be characterised by the full width at half maximum (FWHM) of the bremsstrahlung photon fluence distribution and is represented by a Gaussian distribution (5; 34; 48).

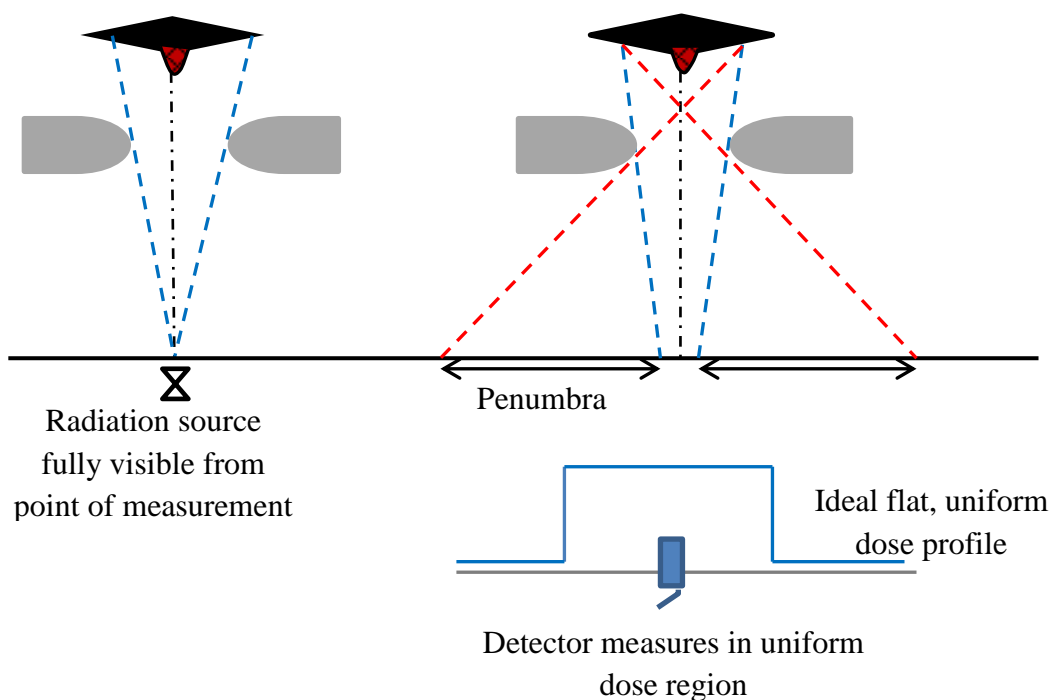


Figure 3.4: The properties of a conventional field. The radiation source is clearly visible at the point of measurement, where the detector is positioned. The dose at the centre of the field is uniform. (45).

As the collimator settings are decreased, the extra-focal radiation contribution becomes less important to the measured dose. The focal spot becomes occluded by the flattening filter or monitor chamber (in case of LINACs) and by the collimating jaws or added multi leaf collimators (in $^{60}\text{Cobalt}$ teletherapy unit and LINACs) when it is viewed at the point of measurement. The primary photons that reach the detector are reduced with decreasing field size. No such reduction occurs for broad fields and the detector receives the full output from the primary beam (63). See Figure 3.5.

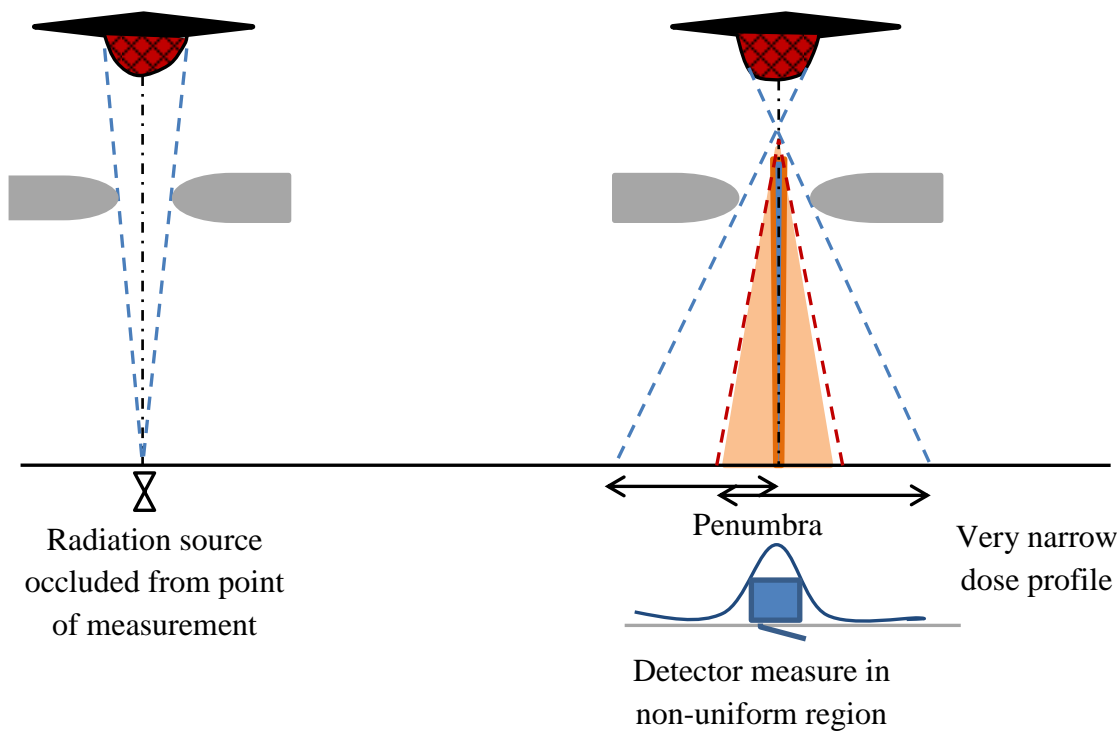


Figure 3.5: Properties of a small field. When the field size is minimised to small field size, the small opening of collimators blocks the extended radiation source partially. The dose at the centre of the small field is non-uniform. (10).

3.3 Charge Particle Equilibrium

When high energy photons interact in a medium, the atoms of the medium are ionized setting into motion high speed primary electrons. These electrons may in turn ionize the surrounding atoms thereby generating secondary electrons (61). Charged particle equilibrium (CPE) or more appropriately termed as electronic equilibrium, is said to exist in a volume (v) in a medium if each electron leaving (v) is replaced by an electron of the same energy entering (v). When the beam radius is small compared to the maximum range of secondary electrons, CPE is lost (20). Figure 3.6 illustrates the concept of CPE when photon beams irradiate a medium.

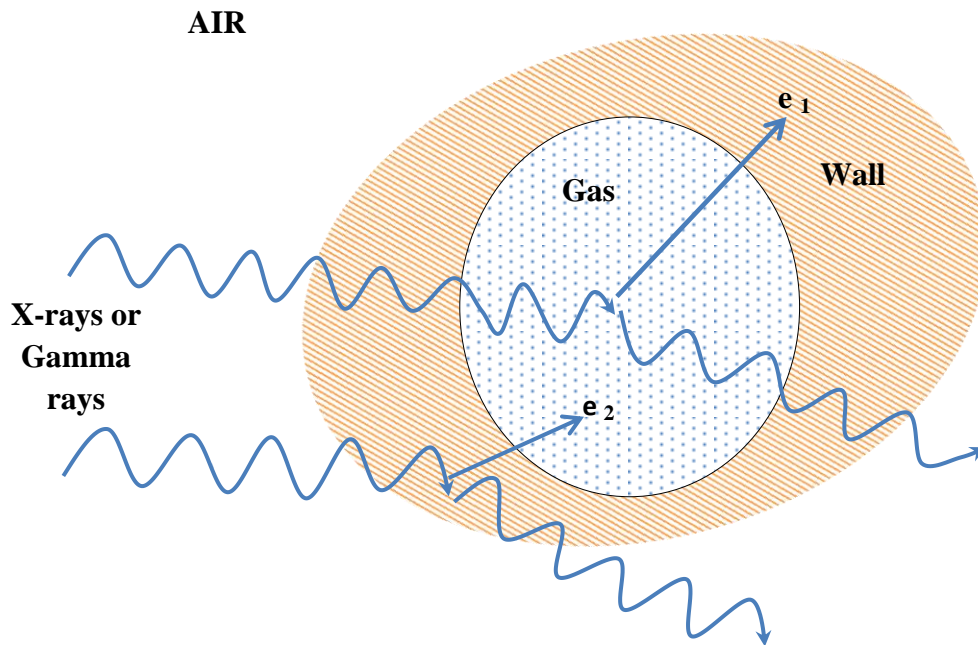


Figure 3.6: The concept of the charged particle equilibrium (CPE). When CPE exists, each charged particle (e_1) carrying energy (E) out of volume with the gas (cavity), the energy lost is compensated by another charged particle (e_2) carrying the same amount of energy into the volume (64).

3.4 Lateral Electronic Equilibrium

Figure 3.5 shows a beam of high-energy photons incident on a medium and illustrates the loss of lateral electronic equilibrium (LEE). The photon beam is assumed to be infinitely sharp, meaning it has zero geometric penumbra (65). “When the incident photons interact with the absorber, point A, well inside the beam, it receives an equal number of electron tracks from the left and from the right. On the other hand point B which is to the right of point A, is still inside the photon beam but receives fewer electrons from the right than from the left. Point B therefore receives a lower dose than point A. Point C is completely outside the photon beam, but still occasionally receives electrons hence the dose there increases from zero to a finite value. Loss of LEE therefore results in an effectively broadened penumbra.

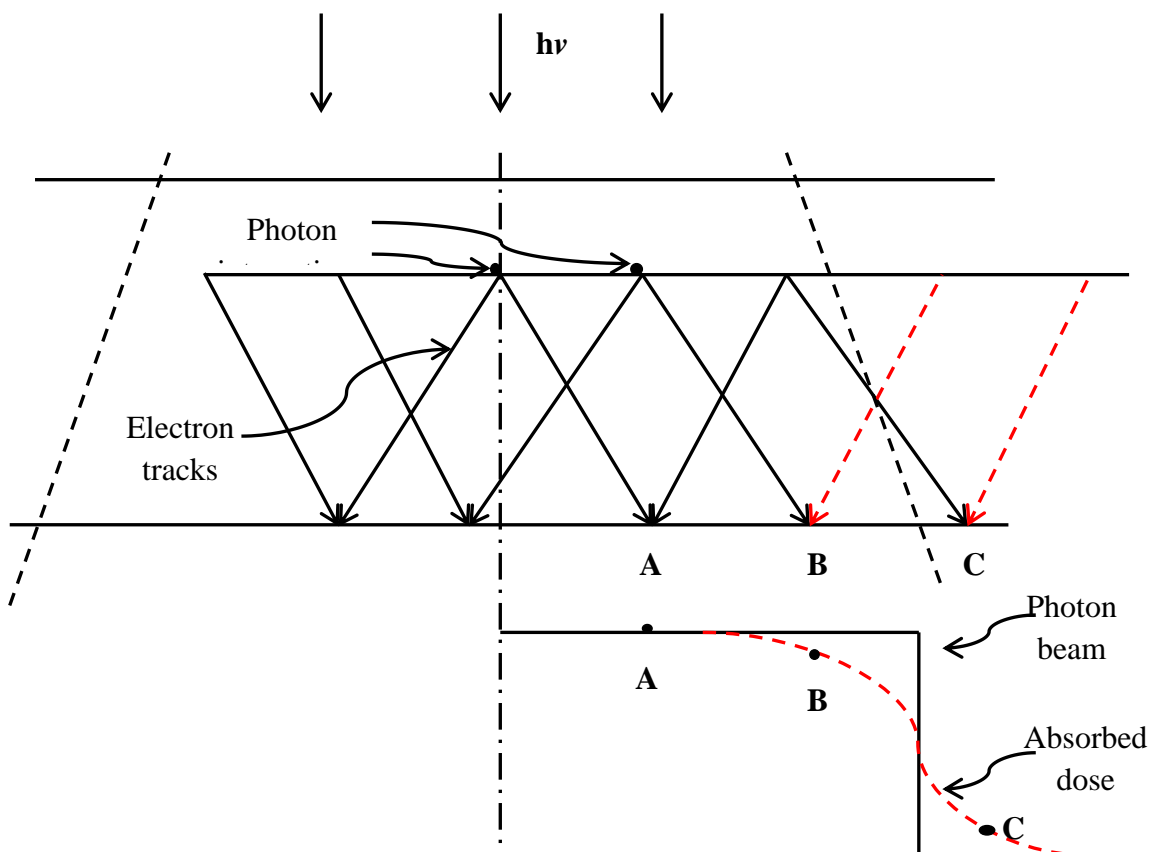


Figure 3.7: The loss of lateral electronic equilibrium (LEE) close to the edge of a high energy photon represented by the dotted lines (34).

At the bottom of Figure 3.7 is a corresponding dose profile for a conventional photon beam. When a photon beam has a small radius, its dose profile not only becomes narrower but it becomes steeper such that the small field photon beam becomes entirely the penumbra, a narrow, steep region of non-uniform dose (34)”.

3.5 Polarity effect

The polarity effect occurs because electrons can be detected on the collecting electrode of the ionization chamber, the chamber stem and sometimes it is because of the ionization chamber-electrometer combination (36; 66). Many ionization chambers show polarity effects from the material used for the collection electrode. Polarity effect can be described as the ratio of the

absolute value of the positive $|\bar{M}_{raw}^+|$ and negative $|\bar{M}_{raw}^-|$ polarity. $|\bar{M}_{raw}|$ is the electrometer reading measured with the polarity used routinely, it can either be positive or negative. Polarity effect can be accounted for by taking measurements at both polarities (43). The polarity correction factor (k_{pol}) can be determined by the following equation:

$$k_{pol} = \frac{|\bar{M}_{raw}^+| + |\bar{M}_{raw}^-|}{2|\bar{M}_{raw}|} \dots\dots\dots 8$$

3.6 Ion recombination and Collection efficiency

Ionization chamber design may result in positive and negative ions in the same track getting recombined. Ionization loss then occurs and this process is known as the ion recombination. At very high ionization intensity such as pulsed beams, high recombination losses occur causing a negative impact on the ion collection efficiency (61). Collection efficiency is the ratio of the number of ions collected to the number of ions produced (67). When operating voltages of an ionization chamber are increased to the saturation point, ion recombination no longer occurs and the ionization chamber is said to be saturated (68).

Lang et al (69) described a method of determining ion collection efficiency. In this method, measurements are made at two unique voltages, one voltage is normally the commonly used operating voltage and the other is a much lower voltage at which ion recombination is likely to occur.

For continuous photon beams such as ⁶⁰Cobalt beams, the ion recombination correction factor can be determined using the relation:

$$k_s = \frac{\left(\frac{V_1}{V_2}\right)^2 - 1}{\left(\frac{V_1}{V_2}\right)^2 - \left(\frac{M_1}{M_2}\right)} \dots\dots\dots 9$$

Where (M_1) and (M_2) are the corrected electrometer readings respectively, with (V_1) being the normal operating voltage and (V_2) is the lowered voltage (43).

3.7 Determination of the small field equivalent square

In order to be able to measure output correction factors for small photon fields, cross-plane and in-plane dosimetric field widths are determined from the Full Width at Half Maximum (FWHM) at the detector measurement depth, i.e. 10 cm. For rectangular small fields with cross-plane and in-plane FWHMs that are not similar, the small field effective square (EQS) is determined by the geometric mean:

$$EQS = \sqrt{A \times B} \dots\dots\dots 10$$

Where A and B are the in-plane and cross-plane dosimetric field widths, defined as the FWHM at the measurement depth (70). The constraint $0.7 < \frac{A}{B} < 1.4$ should be applied when using equation 10.

For circular small field sizes with FWHM radius (r), the following equation is used:

$$EQS = r\sqrt{\pi} = 1.77 \times r \dots\dots\dots 11$$

Where r is the radius of the circular field defined by the points where, on average, the dose levels amounts to 50% of the maximum dose at the measurement depth (70).

Chapter 4. Materials and Methodology

4.1 Types and Properties of Radiation Detectors used.

4.1.1 Ionization Chambers: PTW-31006 pinpoint 0.015 cm³



Figure 4.1: The small-sized PTW 31006 pinpoint 0.015 cm³ therapy chamber for dosimetry in high-energy photon beams that was used in this study.

The pinpoint ionization chamber (shown in Figure 4.1) is recommended for dosimetry in small fields (71). It is used in intensity modulated radiotherapy and stereotactic beams. It has a high spatial resolution and the chamber axis is positioned perpendicular to the incident beam. It is waterproof, fully guarded and can be used in air, solid phantoms and water phantoms.

4.1.2 PTW-31016 3D pinpoint 0.016 cm³



Figure 4.2: An ultra small-sized pinpoint therapy chamber with 3 dimensional characteristics for dosimetry in high-energy photon beams.

The pinpoint 3D ionization chamber (shown in Figure 4.2) is recommended for dose measurements in small fields and is mostly used in Intraoperative radiation therapy (IORT), IMRT and stereotactic beams (72). It has 3 dimensional characteristics which allow it to be used to measure dose in a parallel or perpendicular orientation. It is waterproof, fully guarded and can be utilized in air, solid phantoms and water phantoms (54).

4.1.3 PTW-31010 semiflex 0.125 cm³



Figure 4.3: A PTW 31010 semiflex 0.125 cm³ standard therapy chamber for scanning systems and for relative and absolute dosimetry.

The semiflexible chamber (shown in Figure 4.3) is the perfect compromise between a small size for reasonable spatial resolution and a large sensitive volume. It is one of the most

commonly used chambers in automated beam scanning systems. The sensitive volume is approximately spherical resulting in a flat angular response and a uniform spatial resolution along all three axes of a water phantom (71).

4.1.4 PTW-30013 Farmer 0.6 cm³



Figure 4.4: A PTW 30013 waterproof therapy chamber for absolute dosimetry in high-energy photon, electron and proton beams with sensitive volume of 0.6 cm³, vented to air (54).

Farmer-type ionization chambers (e.g. as shown in Figure 4.4) are one of the most popular used cylindrical ionization chambers for absolute dose measurements in radiation therapy (20). Correction factors needed to determine absorbed dose to water or air kerma are published in the dosimetry CoPs. The PTW 30013 is a waterproof chamber (71). PTW ionization chambers have a calibration traceable to the primary standards of Bureau International de Poids et Mesure (BIPM), Paris (73). In addition, PTW calibration laboratory is recognized internationally as one of the leading Secondary Standard Dosimetry Laboratories in the world (SSDLs) (54).

4.2 Methodology

Routine quality control procedures such as: checking of safety (door interlocks, radiation room monitor), dosimetry (output constancy), mechanical checks (collimator settings, gantry level, cross hair centering) (74) of the unit were carried out before all sets of measurements were performed for this study. The measurements were all performed on an 80 cm source-axis distance (SAD) ⁶⁰Cobalt unit (MDS Nordion Equinox, S/N 2009). This unit had a

minimum square set field size limitation of 1 cm × 1 cm. The gantry alignment was first checked using a spirit level. The ambient pressure and temperature of the water in the phantom were measured using a calibrated Lufft Opus 20 temperature, humidity, air pressure data logger. An automated MP3 water tank (PTW, Freiburg, Germany) of dimensions 60 cm × 70 cm × 50 cm was used. The scanning arm alignment was also checked using a spirit level.

Machine cross hairs were used for the visual initial positioning of the chamber. Each chamber was aligned according to the engineering diagram defining the effective point of measurement. The correct central axis alignment for the Output Factor measurement was determined from the scanning software. Each small field detector was placed at the central axis of the cobalt beam by carefully moving the auto motorized scanning arm of the water tank in ±0.1 mm increments. These movements were done for both the in-plane and cross-plane profiles used to locate the position of the radiation central axis.

Cross calibration of each small field chamber was performed against the calibrated Farmer chamber at a depth of 10 cm at SAD in set fields of 10 cm × 10 cm and the virtual fmsr of 6 cm × 6 cm. The Farmer chamber was calibrated by a secondary standards dosimetry laboratory in absorbed dose to water in a 10 cm × 10 cm field in ⁶⁰Cobalt at a depth of 5 cm. The cross calibration methodology led to the determination of the virtual machine reference field calibration factor ($N_{D,w}$) for the small field detector, which was then used to determine the absolute dose rate in a 4 cm × 4 cm field. Polarity effects and ion recombination measurements were performed and applied to the calculated dose measurements.

Output factors were calculated from the measured relative response of the detectors in series of set field sizes: 10 cm × 10 cm, 6 cm × 6 cm, 4 cm × 4 cm, 3 cm × 3 cm, 2 cm × 2 cm and 1 cm × 1 cm. Three independent setups were done.

The uncertainty budget was produced from the three independent set-ups that were done during the study. Equipment calibration certificates (Type A) and statistical methods (Type B) were used to obtain uncertainties.

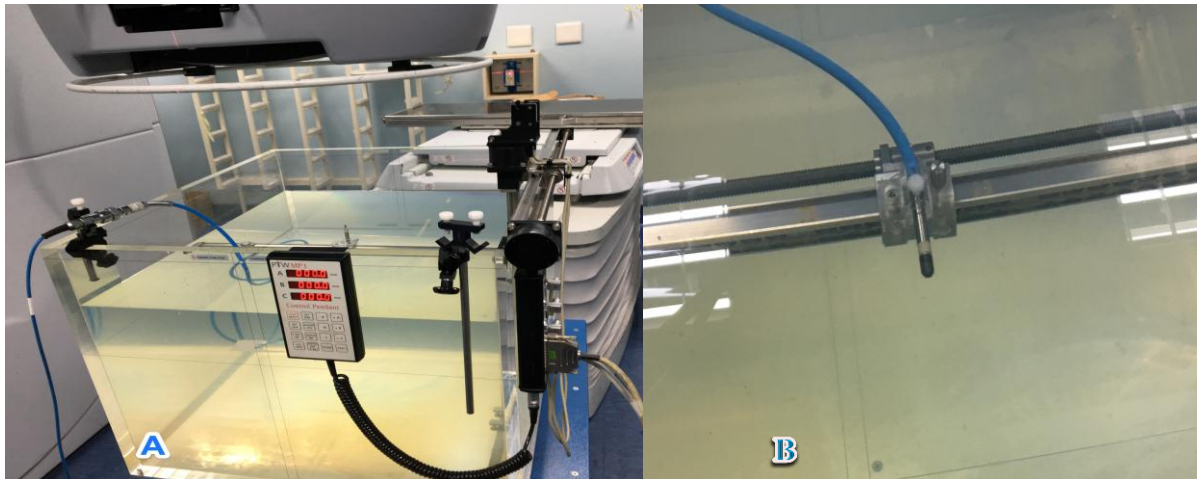


Figure 4.5: The two types of PTW ionization chambers and the PTW MP3 water phantom used to determine the OFs, **A:** PTW 31016 3D pinpoint chamber positioned parallel to the central axis of the beam, **B:** PTW 31010 semiflex chamber positioned perpendicular to the central axis of the beam.



Figure 4.6: A PTW Unidos electrometer that was used to measure the charge, a Lufft Opus 20 temperature, humidity, air pressure data logger device for determining the pressure and the temperature in the room, and the mercury thermometer that was used for measuring the water temperature in the water tank. All these devices were used for measurements during the experiment.

Chapter 5. Results analysis and Discussion

5.1: Dose profiles

Beam profile scans were used to determine the radiation field size which is measured in terms of the full width at half maximum (FWHM). The profile scans therefore assisted in finding the correct positioning of the chambers in all measurement set-ups and in all field sizes. Figures 5.1 - 5.3, show the dose profiles for each chamber for a number of field sizes. The blue lines correspond to in-plane direction profiles and the red lines correspond to cross-plane direction profiles. The ionization chambers were positioned perpendicular to the incident beam at the depth of 10 cm and at an SAD of 80 cm. The PTW 31016 3D pinpoint was however positioned parallel to the central axis of the beam for all measurements.

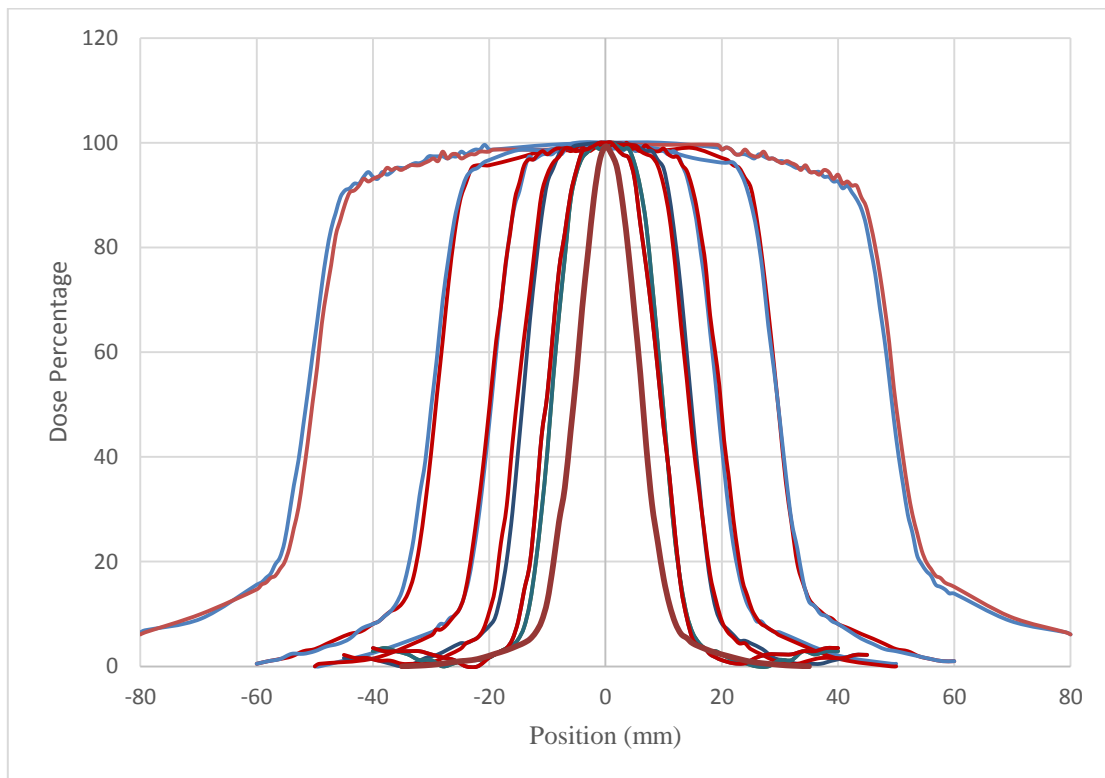


Figure 5.1: In plane (blue lines) and cross plane (red lines) profiles at a depth of 10 cm for field sizes of 10 cm \times 10 cm, 6 cm \times 6 cm, 4 cm \times 4 cm, 3 cm \times 3 cm, 2 cm \times 2 cm and 1 cm \times 1 cm in a $^{60}\text{Cobalt}$ beam using a PTW 31016 3D ionization chamber, positioned parallel to

the central axis of the beam at SAD = 80 cm. The profiles are normalised to the dose at the central axis for each field size.

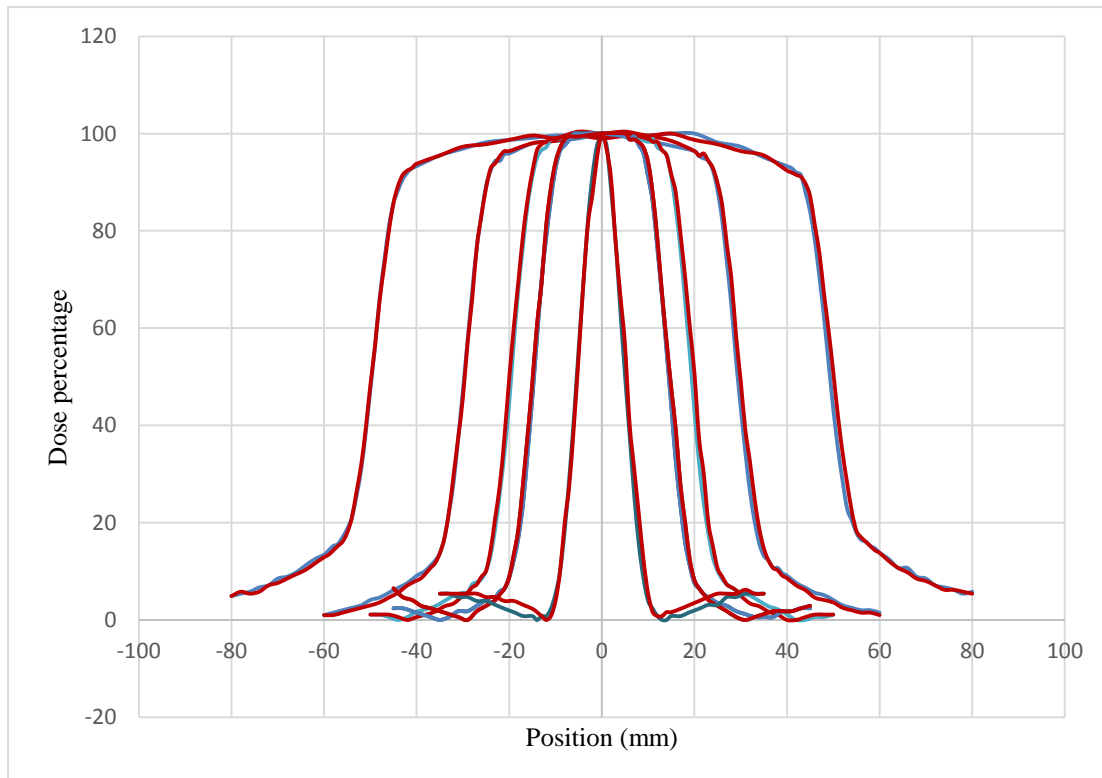


Figure 5.2: In plane (blue lines) and cross plane (red lines) profiles at a depth of 10 cm for field sizes of 10 cm × 10 cm, 6 cm × 6 cm, 4 cm × 4 cm, 3 cm × 3 cm and 2 cm × 2 cm in a ⁶⁰Cobalt beam using a PTW 31006 ionization chamber, positioned perpendicular to the central axis of the beam at SAD = 80 cm. The profiles are normalised to the dose at the central axis for each field size.

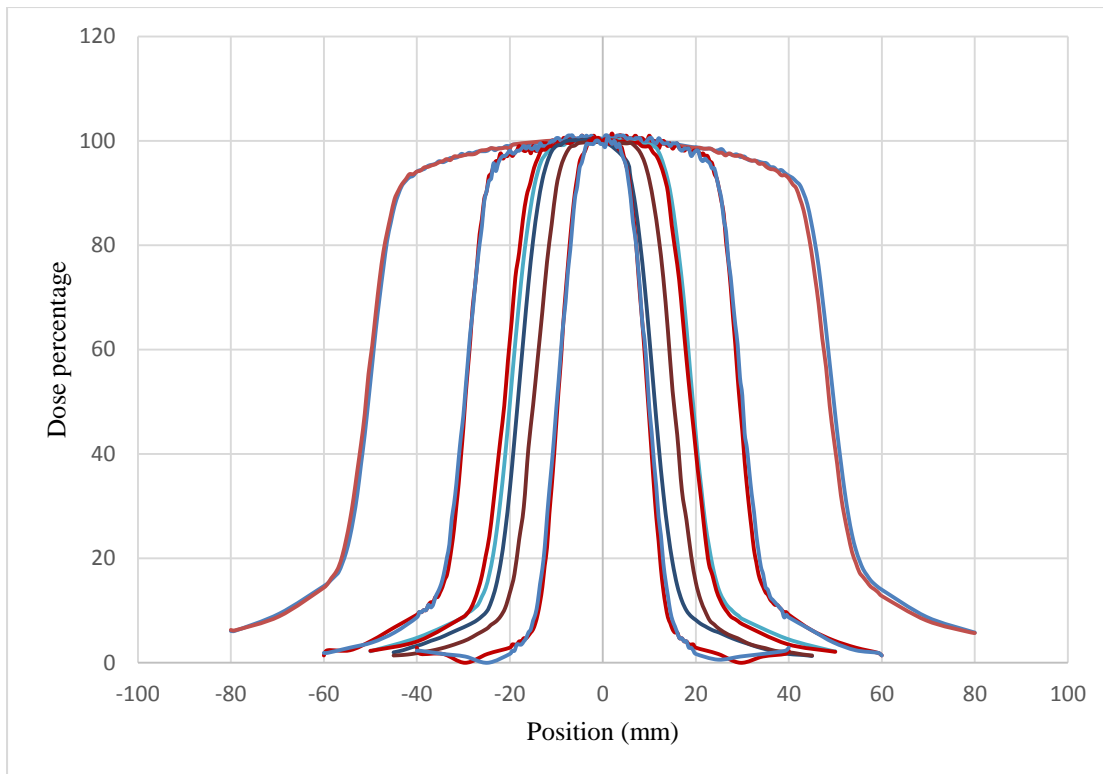


Figure 5.3: In plane (blue lines) and cross plane (red lines) profiles at a depth of 10 cm for field sizes of 10 cm × 10 cm, 6 cm × 6 cm, 4 cm × 4 cm, 3 cm × 3 cm and 2 cm × 2 cm in a $^{60}\text{Cobalt}$ beam using a PTW 31010 ionization chamber, positioned perpendicular to the central axis of the beam at SAD = 80 cm. The profiles are normalised to the dose at the central axis for each field size.

Table 1: Calculations of the effective square fields (ESF) for the set field sizes of 10 cm × 10 cm, 6 cm × 6 cm, 4 cm × 4 cm, 3 cm × 3 cm, 2 cm × 2 cm, and 1 cm × 1 cm using the beam profile scans, for the PTW 31010 semiflex 0.125 cm³, PTW 31006 pinpoint 0.015 cm³ and PTW 31016 3D pinpoint 0.016 cm³ ionization chambers. Cross-plane (A) and in-plane (B) results are shown.

PTW 31010 semiflex 0.125 cm ³	Nominal field size (cm ²)	10		6		4		3		2		1
	Radiation field size (cm ²)	A	B	A	B	A	B	A	B	A	B	--
		9.964	9.968	6.012	6.013	4.002	4.012	2.999	3.001	1.985	2.003	
	A/B	0.9940		0.9969		0.9760		0.9993		0.9905		--
ESF field (cm ²)	9.965		6.012		4.007		3.000		1.899		--	

PTW 31006 pinpoint 0.015 cm ³	Nominal field size (cm ²)	10		6		4		3		2		1	
	Radiation field size (cm ²)	A	B	A	B	A	B	A	B	A	B	A	B
		10.02	9.986	5.942	5.981	3.968	4.000	2.982	3.019	1.993	2.020	1.181	1.206
	A/B	1.003		0.9935		0.9920		0.9877		0.9866		0.9793	
ESF field (cm ²)	10.00		5.961		3.984		3.000		2.006		1.193		

PTW 31016 3D pinpoint 0.016 cm ³	Nominal field size (cm ²)	10		6		4		3		2		1	
	Radiation field size (cm ²)	A	B	A	B	A	B	A	B	A	B	A	B
		9.944	9.988	5.966	6.004	3.953	4.008	2.939	2.965	2.001	1.957	1.063	1.072
	A/B	0.9956		0.9937		0.9863		0.9912		1.022		0.9916	
ESF field (cm ²)	9.966		5.985		3.980		2.952		1.979		1.067		

5.2 Comparison of the Dose Beam Profiles measurements of all detectors

A comparison of the dose profiles obtained from the three chambers namely PTW 31016 3D, PTW 31006, and PTW 31010 is shown in Figures 5.4 - 5.8 for different field sizes. Chambers were positioned at the depth of 10 cm and at a SAD of 80 cm. The dose profiles show an agreement between the three detectors for the fields of 10 cm × 10 cm, 6 cm × 6 cm, 4 cm × 4 cm. At 2 cm × 2 cm fields the PTW 31010 shows a broadened penumbra (see from Figures 5.6 and 5.7. The FWHM (50% of the dose percentage) obtained from the profiles was consistent.

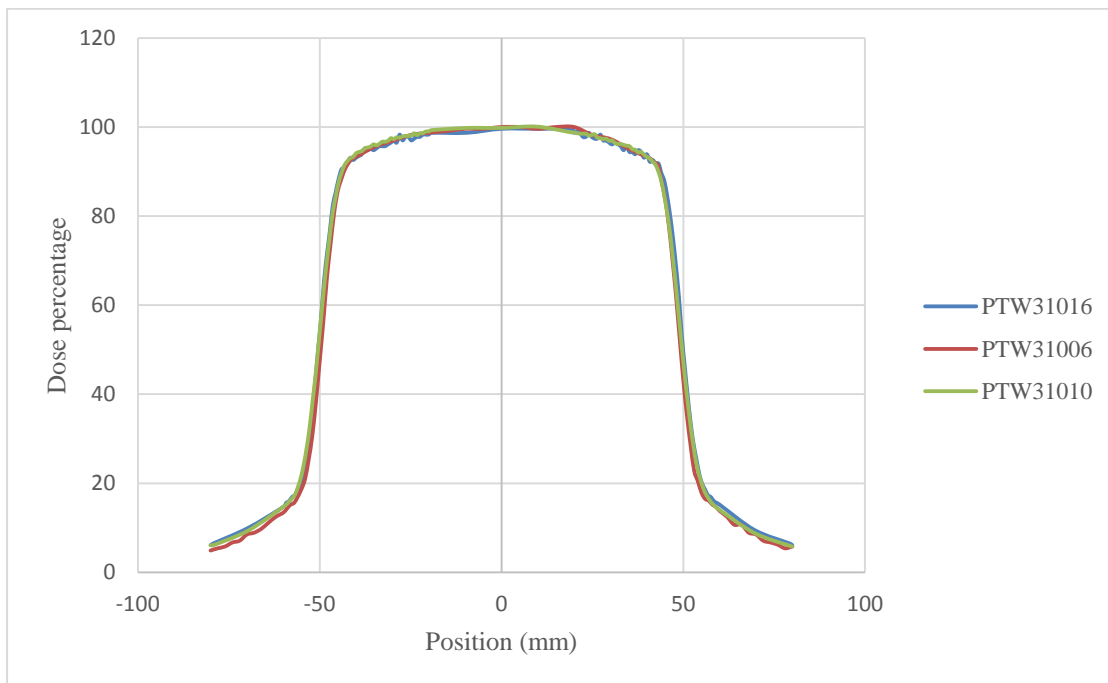


Figure 5.4.: The dose profiles taken in a water tank from a ^{60}Co Cobalt photon beam. The field size was set to 10 cm × 10 cm, at a depth of 10 cm and at a SAD of 80cm . The ionization chambers used were: PTW 31016 (Blue), PTW 31006 (Red) and PTW 31010 (Green).

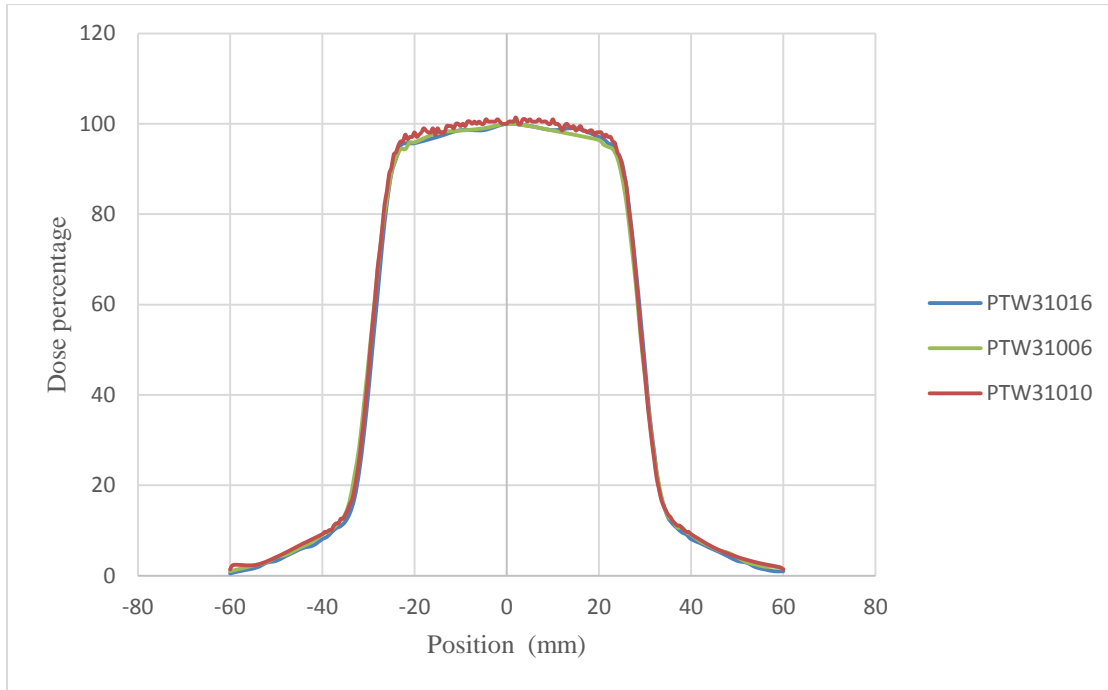


Figure 5.5: The dose profiles taken in a water tank from a $^{60}\text{Cobalt}$ photon beam. The field size was set to $6\text{ cm} \times 6\text{ cm}$, at a depth of 10 cm and at a SAD of 80cm. The ionization chambers used were: PTW 31016 (Blue), PTW 31006 (Green) and PTW 31010 (Red).

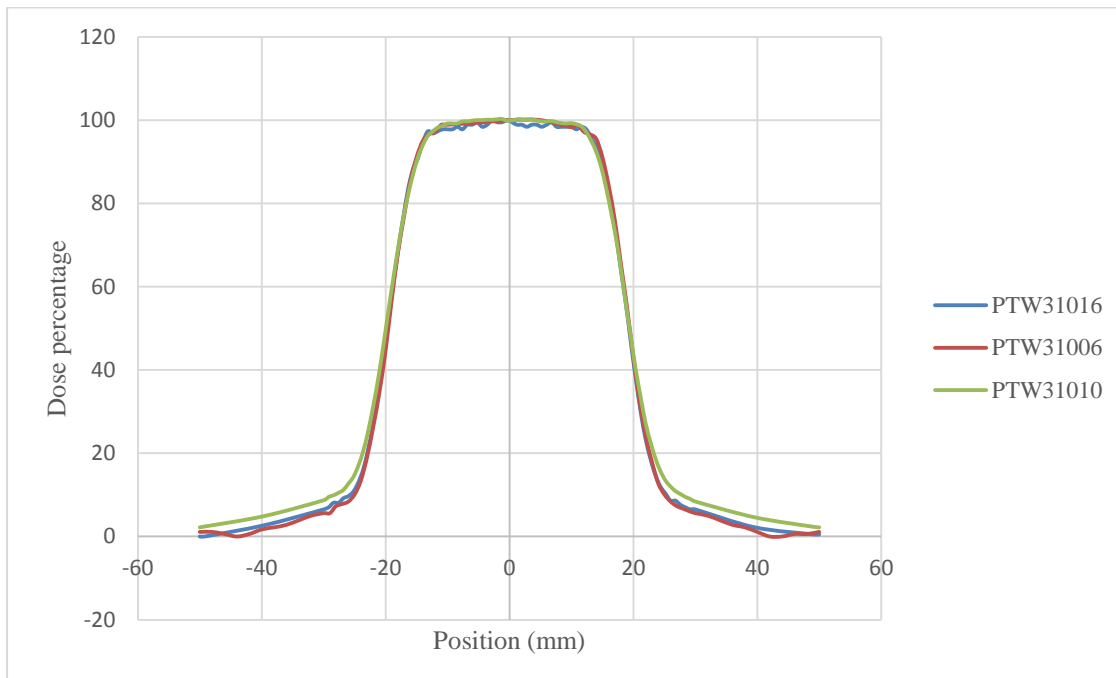


Figure 5.6: The dose profiles taken in a water tank from a $^{60}\text{Cobalt}$ photon beam. The field size was set to $4\text{ cm} \times 4\text{ cm}$, at a depth of 10 cm and at a SAD of 80cm. The ionization chambers used were: PTW 31016 (Blue), PTW 31006 (Red) and PTW 31010 (Green).

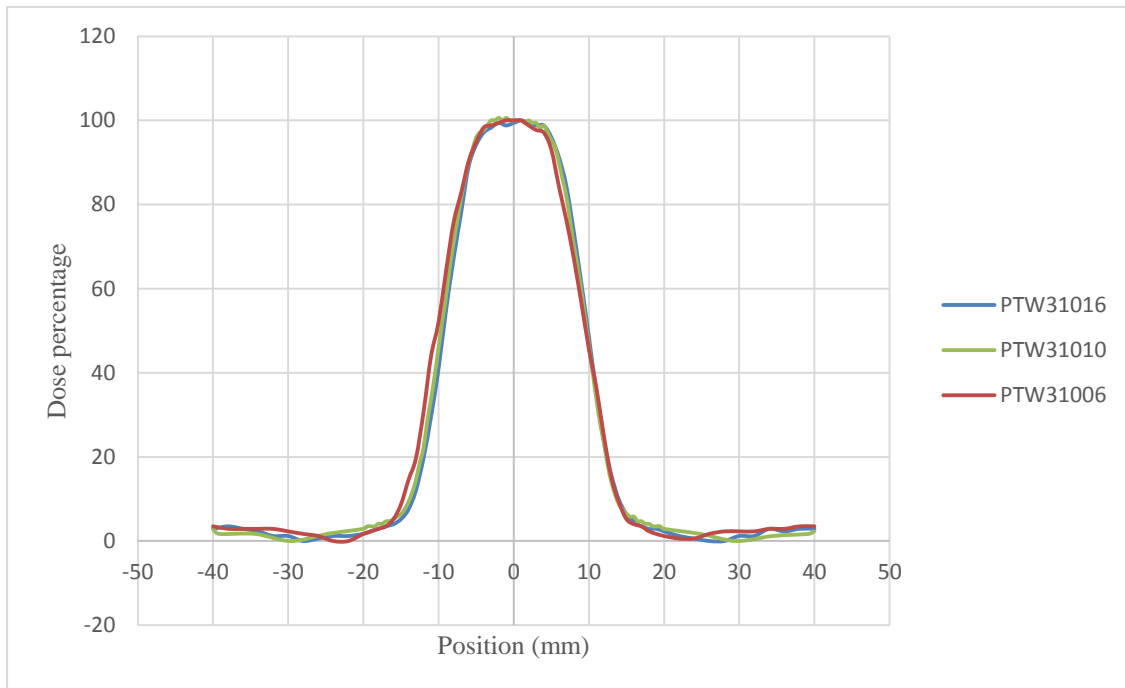


Figure 5.7: The dose profiles taken in a water tank from a $^{60}\text{Cobalt}$ photon beam. The field size was set to $2\text{ cm} \times 2\text{ cm}$, at a depth of 10 cm and at a SAD of 80cm. The ionization chambers used were: PTW 31016 (Blue), PTW 31006 (Red) and PTW 31010 (Green).

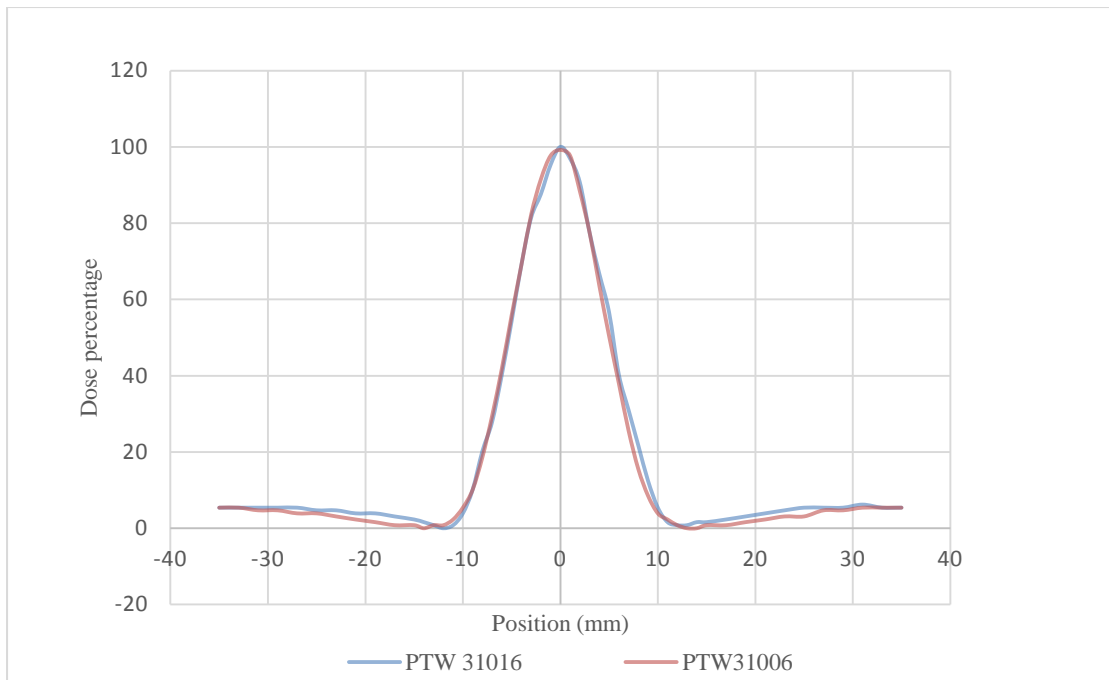


Figure 5.8: The dose profiles taken in a water tank from a ^{60}Co photon beam. The field size was set to $1\text{ cm} \times 1\text{ cm}$, at a depth of 10 cm and at a SAD of 80 cm . The ionization chambers used were: PTW 31016 (Blue), and PTW 31006 (Red).

5.3 Cross calibration

The small field ionization chambers (PTW 31016 3D pinpoint 0.016 cm^3 , PTW 31006 pinpoint 0.015 cm^3 and PTW 31010 semiflex 0.125 cm^3) were cross calibrated against a PTW 30013 Farmer chamber in a $6\text{ cm} \times 6\text{ cm}$ virtual msr field at a depth of 10 cm at 80 cm SAD. The measured dose to water calibration factors were compared with the chamber calibration certificate.

Table 2 below shows the results obtained.

Table 2: Cross calibration results of the small field chambers at 6 cm × 6 cm field size calibrated against the PTW M 30013 0.6 cm³ Farmer chamber with their uncertainties.

Chamber	N_{DW} (Calculated) Gy/nC	Perc Difference (%Δ)	Uncertainty (A)
PTW 31016 3D (Parallel)	2.358	2.169	0.00025
PTW 31016 3D (perpendicular)	2.367	1.768	0.00013
PTW 31006 pinpoint	2.466	1.357	0.000062
PTW 31010 pinpoint semiflex	0.3017	5.887	0.0000

5.4 Daisy Chain method

The daisy chain method (indirect method) was employed in this work in order to determine the dose rate in a 4 cm × 4 cm field using the calibration obtained from the 6 cm × 6 cm msr field. The polarity effect and ion recombination correction factors were applied to the daisy chain results. Table 3 shows the results obtained.

Table 3: Dose rate data obtained from the daisy chain measurements on 02/08/2016 in a field of 4 cm × 4 cm using a PTW 30013 0.6 cm³ Farmer, PTW 31016 3D pinpoint, PTW 31006 pinpoint 0.015 cm³ and PTW 31010 semiflex 0.125 cm³ chamber. The measurements were performed at the depth of 10 cm, SAD of 80 cm in a water phantom.

Chamber	Dose rate at Dmax (cGy / min)
	4 × 4 cm ²
PTW 30013 Farmer	59.74 + 0.35
PTW 31016 3D pp	59.82 ± 0.33
PTW 31006 pp	60.41 ± 0.34
PTW 31010 semiflex	61.11 ± 0.35

5.5 Relative Output Factors

5.5.1: Comparison of Relative Output Factor Measurements from all Detectors

Figure 5.8 below shows the uncorrected output factors obtained from the relative response of each of the detectors. The relative output factors are normalized at the 10 cm × 10 cm field. The response of the PTW 31006 pinpoint 0.015 cm³ ionization chamber and the PTW 31016 3D pinpoint 0.016 cm³ is reduced in the 1 cm × 1 cm field. This reduction can be associated to the lack of electronic equilibrium and dose averaging effect by the sensitive volume of these detectors at small field sizes. In order to get correct results, it is necessary to apply

correction factors that will account for the effects associated with the field and detector size. The PTW 31010 semiflex 0.125 cm³ was not used in the 1 cm × 1 cm field because of its large size in comparison to the field. Interpolated British Journal of Radiology (BJR) supplement 25 (2) output factors are also shown. There is a substantial deviation between the BJR published data and the relative output factors at all field sizes.

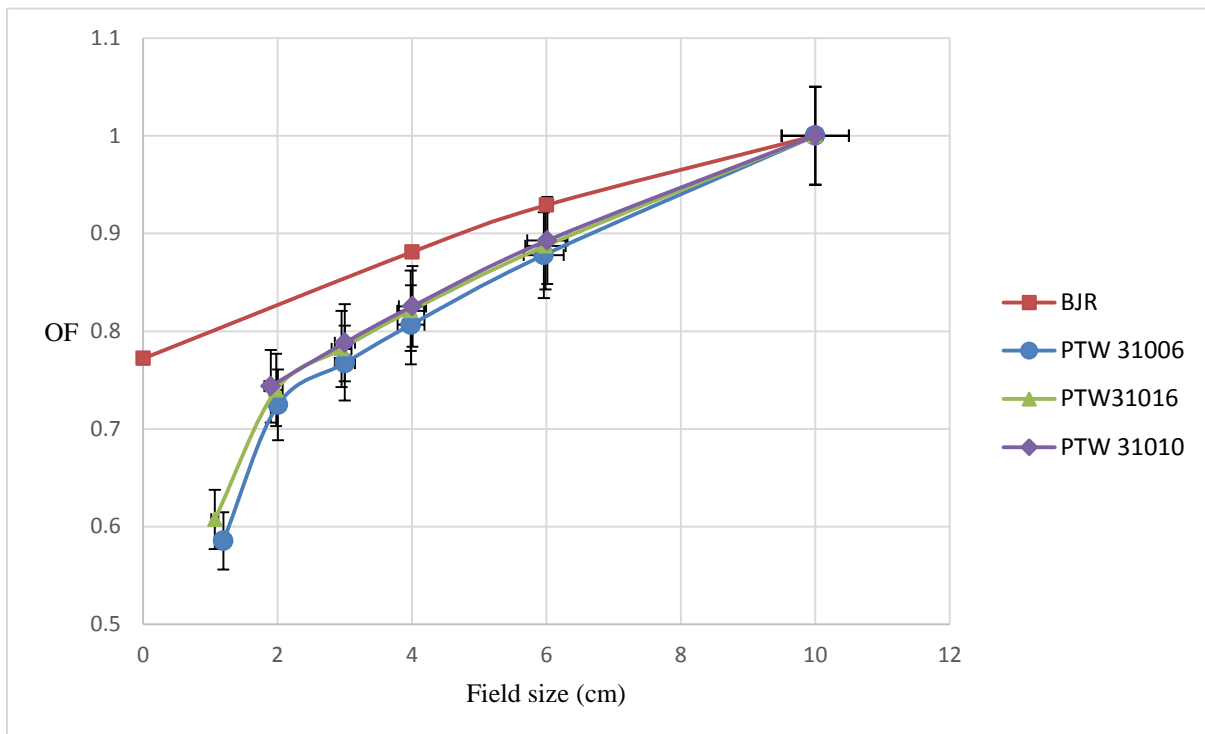


Figure 5.9: Comparison of the relative output factors from the PTW 31006 pinpoint 0.015 cm³, PTW 31016 3D pinpoint 0.016 cm³ and PTW 31010 semiflex 0.125 cm³ with the BJR supplement 25 ⁶⁰Cobalt published data as a function of field size. The data are normalized to the field size of 10 cm × 10 cm. Error bars are shown for the measured data series and represent the percentage error with 5% value.

5.7: Uncertainty Budget

The uncertainty budget was produced from the three independent set-ups that were done during the study. Equipment calibration certificates were used to obtain some uncertainties. Type A uncertainties are the uncertainties calculated using statistical methods. Type B uncertainties are determined from other methods, e.g. calibration certificates, equipment resolution, zero offset, installation, etc. See table 4 for uncertainty budget.

Table 4: Uncertainty budget with the type A and type B uncertainties for PTW 31010, PTW 31006 and PTW 31016 3D small field ionization chambers. The percentage difference was 1.13% between the independent setups for which the output factors were calculated.

Source	Estimated	Type
Detector Calibration	3,300%	B
Thermometer Calibration	0,1250%	B
Thermometer Resolution	0,002500%	B
Barometer Calibration	0,1250%	B
Barometer Resolution	0.05000%	B
Dose calibration	0.3000%	A
Daisy chain (setup 1, 2 & 3 combined)	0.3400%	A
Polarity	0.04258%	A
Ion recombination	0.0002374%	A
Output factor uncertainties (setup 1, 2 & 3)	1.120%	A
Dose rate	0.6000%	A
Combined Standard Uncertainty 95 % confidence, K = 2	3,390%	

Chapter 6. Conclusions

Small field dosimetry in a ^{60}Co photon beam using three different models (31010, 31006, 31016) of PTW small field ionization chambers was investigated. The field sizes were created using the secondary collimators of the ^{60}Co unit. SAD technique was used and all measurements were performed at 70 cm source-surface distance and at a depth of 10 cm in water.

The radiation field size was determined using in-plane and cross-plane beam profile scans. The FWHM of the profiles were used to determine the effective square field (ESF) for the three ionization chambers. The ionization chambers were initially positioned such that the cross wire was at the geometrical point of measurement as defined by the engineering diagram. The actual point of measurement of the detectors determined from beam profile scans was found to be different from the engineering diagrams.

A cross calibration was performed for the three small field ionization chambers against a calibrated PTW M30013 0.60 cm^3 Farmer chamber to achieve traceability. A virtual fmsr field of $6\text{ cm} \times 6\text{ cm}$ was used for the cross calibrations. The dose rate was then determined in a $4\text{ cm} \times 4\text{ cm}$ field using the daisy chain method, and the dose rate obtained from all the ionization chambers was $60.27 \pm 0.34\text{ cGy/min}$.

Relative output factors were then measured with the three detectors for set field sizes of $10\text{ cm} \times 10\text{ cm}$, $6\text{ cm} \times 6\text{ cm}$, $4\text{ cm} \times 4\text{ cm}$, $3\text{ cm} \times 3\text{ cm}$, $2\text{ cm} \times 2\text{ cm}$ and $1\text{ cm} \times 1\text{ cm}$. For the PTW 31010 the measurements were not done at $1\text{ cm} \times 1\text{ cm}$. For fields larger than $2\text{ cm} \times 2\text{ cm}$, the percentage difference between the output factors measured with the three ionization chambers was $\pm 0.81\%$. When comparing the relative output factors, the PTW 31010 pinpoint 0.125 cm^3 and PTW 31016 3D pinpoint 0.016 cm^3 were in close agreement for field sizes of $2\text{ cm} \times 2\text{ cm}$, $4\text{ cm} \times 4\text{ cm}$ and $6\text{ cm} \times 6\text{ cm}$. Field output correction factors may be required for these ionization chambers in field sizes under $2\text{ cm} \times 2\text{ cm}$, however more data needs to be obtained from another detector, e.g. a solid state, film or liquid ionization chamber, in order to confirm this.

The BJR ^{60}Co data should not be used in small field sizes and should be treated with care. Broad field dosimetry data cannot be extrapolated to small and non-standard field sizes or to modern teletherapy units.

Chapter 7. References

1. **International Atomic Energy Agency & American Association of Physicists in Medicine.** *Dosimetry of Small Static Fields Used in External Beam Radiotherapy. An International Code of Practice for Reference and Relative Dose Determination prepared jointly with the IAEA and AAPM.* Vienna : IAEA, In press.
2. **Aird EGA, Burns JE, Day MJ, Duane S, Jordan TJ, Kacperek A, et al.** *BJR Supplement 25 Central Axis Depth Dose Data for Use in Radiotherapy:1996.* London : British Institute of Radiology, 1996. 0 905749 38 3.
3. **UK, Cancer Research.** Cancer Research UK. *Cancer Research UK website.* [Online] Dec 10, 2016. [Cited: Jan 23, 2017.] <http://www.cancerresearchuk.org/health-professional/cancer-statistics/survival>.
4. **H, Badakhshi.** *Image Guided Stereotactic Radiosurgery-High precision,Non-invasive Treatment of Solid Tumors.* Switzerland : Springer International Publishing, 2016. 978-3-319-39189-2.
5. *Dose measurements in small fields.* **JU, Wuerfel.** 1, s.l. : Medical Physics International Journal, 2013, Vol. 1.
6. *Small fields nonequilibrium radiation dosimetry.* **Das I, Ding G, Ahnesjo A.** 1, Philadelphia : Med.Phys, 2008, Vol. 35. 10.1118/1.2815356.
7. **Aspradakis MM, Byrne JP, Palmans H, Duane S, Conway J, Warrington AP et al.** *Small Field MV Photon Dosimetry, Report No 103.* London : Institute of Physics and Engineering in Medicine, 2010. 9781903613450.
8. *Dosimetry of small photon beams used for stereotactic radiosurgery/radiotherapy.* **Dieterich S, Cavedon C, Wilcox E.** Vicenza : Stanford School of Medicine.
9. **Hendee WR, Benedict SH, Schlesinger DJ, Goetsch SJ, Kavanagh BD.** *Stereotactic Radiosurgery and Stereotactic Body Radiation Therapy.* London New York : CRC Press, 2015. 13: 978-1-4398-4198-3.
10. **Aspradakis M, Byrine J.** Medical Physics web. *Medical Physics website.* [Online] Mar 8, 2011. [Cited: 12 05, 2016.] <http://medicalphysicsweb.org/cws/article/opinion/45334>.
11. **Thariat J, Hannoun-Levi J, Myint A, Gerard J.** Oregon Health & Science University. *Oregon Health & Science University website.* [Online] 2001 - 2016. [Cited: May 20, 2016.] http://www.ohsu.edu/xd/education/schools/school-of-medicine/departments/clinical-departments/radiation-medicine/education-training/upload/PastPresentFuture_RT_review_Thariat2012.pdf.

12. The National Institute of Mental Health. *The National Institute of Mental Health web site*. [Online] [Cited: December 16, 2016.] <https://www.nimh.nih.gov/health/statistics/suicide/leadingcausesofdeaths185inthe-us.shtml>.
13. *Has the time come for doing away with Cobalt60 teletherapy for cancer treatments* . **R, Ravichandran**. 34, Oman : J Med Phys, 2009, Vol. 2. 10.4103/09716203.51931.
14. **Cherry S, Sorenson J, Phelps M**. *Physics in Nuclear Medicine*. Philadelphia : Elsevier Saunders, 2012. 978-1-4160-5198-5.
15. **U, Linz**. *Ion Beam Therapy Fundamentals, Technology, Clinical Applications*. London : Springer-Verlag Berlin Heidelberg, 2012. 978-3-642-21413-4.
16. *Nuclear physics and particle therapy* . **Battistoni G, Mattei I, Muraro S**. 4, s.l. : Advances in Physics, 2016, Vol. 1. 10.1080/23746149.2016.1237310.
17. *Nuclear physics in particle therapy: a review*. **Durante M, Paganetti H**. 79, Boston : Iopscience, 2016. 10.1088/0034-4885/79/9/096702.
18. *Determination of output factors for small proton therapy fields*. **Fontenot JD, Newhauser WD, Bloch C, White RA, Titt U, Starkschall G**. 34, s.l. : Med Phys, 2007, Vol. 2. 10.1118/1.2428406.
19. *Dosimetric consistency of Co-60 teletherapy unit*. **Baba M, Mohib-ul-Haq M, Khan A**. 1, Jammu and Kashmir : IJHS, Jan 07, 2013, Vol. 7. PMC3612411.
20. **EB, Podgorsak**. *Radiation Oncology Physics: A Handbook for Teachers and Students*. Vienna : IAEA, 2005. 92–0–107304–6.
21. *A comparison between cobalt and linear accelerator based treatment plans for conformal and intensity modulated radiotherapy*. **Adams EJ, Warrington AP**. 964, s.l. : Br J Radiol, 2008. 10.1259/bjr/77023750.
22. **P, Petti**. Gamma Knife. *AAPM website*. [Online] 2009. [Cited: June 12, 2016.] <http://amos3.aapm.org/abstracts/pdf/68-19901-237350-85912.pdf>.
23. *Teletherapy sources with imported and indigenous Co-60 activity*. **George J, Kushwah R, Sastry K**. 3, Navi Mumbai : J Med Phys, 2009, Vol. 34. 10.4103/09716203.54854.
24. **D, Pantalony**. Introduction to Teletherapy and Cobalt Mechine. *Slideshare website*. [Online] Dec 04, 2011. [Cited: May 20, 2016.] <http://www.slideshare.net/abishadh/cobalt60-external-beam-radiation-therapy>.
25. **Jayarajan K, Kar D, Radke M, Singh M**. Bhabha Atomic Research Centre. *Bhabha Atomic Research Centre website*. [Online] Dec 2, 2016. [Cited: Dec 5, 2016.] <http://www.barc.gov.in/publications/nl/2005/200502-2.pdf>.

26. **Albino D, Ale D, Easa A, Mayeeshiba M, Straka A, Traverse A.** *Criteria for teletherapy unit change.* s.l. : University of Wisconsin Madison, 2015.
27. *Cobalt, Linac, or Other: What is the best solution for Radiation Therapy in developing countries?* **Brandi RP, Alana DH, Derek WB, Adam CS, May A, Brandon JF, Shilpen P.** 3, Washington : Int J Radiation Oncol Biol Phys, 2013, Vol. 89. 10.1016/j.ijrobp.2013.12.022.
28. *Practical and clinical consideration in Cobalt-60 tomotherapy.* **Joshi C, Dhanesar S, Darko J, Kerr A, Vidyasaga P, Schreiner L.** 3, Ontario : J Med Phys, 2009, Vol. 34. 10.4103/09716203.54847.
29. **Human Health, IAEA.** *Planning National Radiotherapy Services: A Practical Tool.* Vienna : IAEA, 2010. Series No 14 / 978-92-0-105910-9.
30. *Dosimetry tools and techniques for IMRT.* **Daniel L, Jean M, James D, Lei D, Mark O.** 3, Missouri : Med. Phys., 2011, Vol. 38. 10.1118/1.3514120.
31. **DA, Guerra.** *Ionizing Radiation Detectors for Medical Imaging.* London : World Scientific Publishing Co.Pte.Ltd, 2004. 981-238-674-2.
32. **K, Dumela.** *Optimizing patient protection during diagnostic procedures-developing diagnostic reference levels at the Dr George Mukhari Hospital.* Pretoria : University of Limpopo, 2010.
33. **AC, Chamberlain.** *Thermoluminescent Dosimetry Practical.* Pretoria : University of Limpopo, 2005.
34. **A, Bacala.** *Measurements of output factors for small photon fields up to 10 cm x 10 cm .* Florida : Florida Atlantic University, 2013.
35. **H, Bouchard.** NPL. *NPL web site.* [Online] Jan 2016. [Cited: Oct 14, 2016.] <http://www.npl.co.uk/upload/pdf/pcrd-14-notes.pdf>.
36. **Symonds P, Deehan C, Mills J, Meredith C.** *Walter and Millers Textbook od Radiotherapy.* London : Elsevier Ltd, 2012. 978 0 443 07486 8.
37. *The energy dependence and dose response of a commercial optically stimulated luminescent detector for kilovoltage photon, megavoltage photon and electron, proton and carbon beams.* **S, Chester.** 5, Chicago : Am. Assoc. Phys. Med., 2009, Vol. 36. 10.1118/1.3097283.
38. **H, Palmans.** National Physical Laboratory. *National Physical Laboratory website.* [Online] May 13, 2014. [Cited: Jul 27, 2016.] <http://www.npl.co.uk/upload/pdf/20140513-dart-pres-palmans-2.pdf>.
39. **A, Arlebrand.** *Dosimetric characteristics of CVD single crystal diamond detectors in radiotherapy beams.* Stockholm : Stockholm University, 2007.

40. **C, Orton.** *Radiation Dosimetry Physical and Biological Aspects.* Michigan : Springer Science+Business Media New York, 1986. 978-1-4899-0571-0.
41. **FH, Attix.** *Introduction to Radiological Physics and Radiation dosimetry.* Weinheim : WILEY-VCH Verlag GmbH & Co. KGaA , 2007. 978-0-471-01 146-0.
42. **Dieterich S, Ford E, Pavord D, Zeng J.** *Practical Radiation Oncology Physics.* Philadelphia : Elsevier, Inc, 2016. 978-0-323-26209-5.
43. **International Atomic Energy Agency Technical Report Series No.398.** *Absorbed Dose Determination in External Beam Radiotherapy: An International Code of Practice for Dosimetry based on Standards of Absorbed Dose to Water.* Vienna : IAEA, 2006. 1011-4289.
44. *The influence of small field sizes, penumbra, spot size and measurement depth on perturbation factors for microionization chambers.* **Crop F, Reynaert N, Pittomvils G, Paelinck L, De Wagter C, Thierens C.** 9, Gent : Phys. Med. Biol., 2009, Vol. 54. 10.1088/0031-9155/54/9/024.
45. **J, Seuntjens.** The American Association of Physicists in Medicine. *AAPM webcite.* [Online] Apr 07, 2011. [Cited: Jul 29, 2016.] <http://chapter.aapm.org/seaapm/meetings/2011/S4-T1-Suentjens-Small-Field-Dosimetry.pdf>.
46. *A new formalism for reference dosimetry of small and non standard fields.* **Alfonso R, Andreo P, Capote R, Saiful Huq M, Kilby W, Kjall P, et al.** 11, La Habana : Med.Phys., 2008, Vol. 35. 10.1118/1.3005481.
47. **Almond P, Biggs PJ, Coursey BM, Hanson WF, Huq MS, Nath R, et al.** *AAPM's TG-51 protocol for clinical reference dosimetry of high energy photon and electron beams.* Virginia : Med. Phys. 26, 1999. 1847-1870.
48. **Aspradakis MM, Byrine JR, Palmans H, Duane S, Conway J, Warrington AP, Rosser K.** IAEA. *IAEA web site.* [Online] Dec 15, 2016. [Cited: Dec 16, 2016.] https://inis.iaea.org/search/search.aspx?orig_q=RN:42026432.
49. *Challenges in small field MV photon dosimetry.* **MM, Aspradakis.** Lucerne : Luzerner Kantonsspital, 2010.
50. **International Atomic Energy Agency.** IAEA. *IAEA website.* [Online] Sep 03, 2015. [Cited: Aug 02, 2016.] <http://cra.iaea.org/crp/project/ProjectDetail?projectId=2061&lastActionName=OpenedCRPList>.
51. *Determination of the correction factors for different ionization chambers used for the calibration of the helical tomotherapy static beam.* **Zeaverino M, Agostinelli S, Pupillo F, Taccini G.** 2011, Genoa : Elsevier Ireland Ltd, 2011, Vol. 100. 10.1016/j.radonc.2011.08.044.

52. **Rogers D, Joanna C.** *Clinical Dosimetry Measurements in radiotherapy.* s.l. : AAPM, 2009. 9781888340839.
53. **Freiburg, PTW.** PTW Freiburg. *PTW Freiburg website.* [Online] Sep 21, 2016. [Cited: Dec 05, 2016.] http://www.ptw.de/fileadmin/data/download/catalogviewer/Small_Field_Application_Guide_92020000_05/blaetterkatalog/blaetterkatalog/pdf/complete.pdf.
54. —. PTW Freiburg. *PTW Freiburg website.* [Online] Sep 21, 2016. [Cited: Dec 05, 2016.] http://www.ptw.de/1818.html?&no_cache=1&tx_bitptwdwlplus_pi1%5Bid%5D=data_2&tx_bitptwdwlplus_pi1%5Bpdf%5D=c958863e0cc5626e47103e0760c0f4eb.
55. *Lateral electron equilibrium and electron contamination in measurements of head-scatter factors using miniphantoms and brass caps.* **Li A, Soubra M, Szanto J, Gerig L.** 7, Ontario : Med.Phys, 1995, Vol. 22. 0094-2405/95/22(7).
56. *Characterizing the influence of detector density on dosimeter response in non-equilibrium small photon fields.* **Scott AJ, Kumar S, Nahum AE, Fenwick JD.** 14, Bebington Wirral : Med.Phys.Biol, 2012, Vol. 57. 10.1088/0031-9155/57/14/4461.
57. *The effect of air cavity size in cylindrical ionization chambers on the measurements in high-energy radiotherapy photon beams—an experimental study.* **Swanpalmer J, Johansson KA.** 14, Gothenburg : Med.Phys.Biol, 2012, Vol. 57. 10.1088/0031-9155/57/14/4671.
58. *calculation of correction factors for ionization chamber measurements with small fields in low density media.* **Pisature O, Pachoud M, Bechud FO, Moeckli R.** 14, Lausanne : Med.Phys.Biol, 2010, Vol. 57. 10.1088/0031-9155/57/14/45.
59. *Flattening filterfree accelerators: a report from the AAPM Therapy Emerging Technology Assessment Work Group.* **Xiao Y, Kry S, Poppo R, Yorke E, Papanikolaou N, Stathakis S, et al.** 3, Philadelphia : JACMP, 2015, Vol. 16.
60. **KS, Reddy.** Ministry of Health and Family welfare. *Ministry of Health and Family welfare web site.* [Online] 01 02, 2017. [Cited: 01 05, 2017.] <http://www.mohfw.nic.in/WriteReadData/1892s/Choice%20Of%20A%20Teletherapy%20Unit.pdf>.
61. **F, Khan.** *Physics of Radiation Therapy, The, 4th Edition.* Minnesota : Lippincott Williams & Wilkins, 2010.
62. **Khan F, Gibbons J.** *Khan's The Physics of Radiation Therapy.* Philadelphia : Lippincott Williams and Wilkins, 2014. 978-1-4511-8245-3.
63. **Beddar S, Beaulieu L.** *Imaging in Medical diagnosis and therapy: Scintillation Dosimetry.* Boca Raton : CRC Press, 2016. 13: 978-1-4822-0900-6.
64. Oregon State University. *Oregon State University website .* [Online] 2004. [Cited: Nov 02, 2016.] <https://courses.ecampus.oregonstate.edu/ne581/five/>.

65. **Dieterich S, Cavedon C, Wilcox E.** Dosimetry of Small Photon Beams Used for Stereotactic Radiosurgery/Radiotherapy. [book auth.] Cygler JE Rogers DWO. *Clinical Dosimetry Measurements in Radiotherapy*. Vicenza : AAPM, 2009.
66. *Polarity effect in commercial ionization chambers used in photon beams with small fields.* **T, Shimono, et al., et al.** Osaka : Radiol Phys Technol , 2009, Vol. 2. 10.1007/s12194-008-0050-1.
67. **Larry A, Davis S, Bartol L, Grenzow F.** American Association of Physicists in Medicine. *American Association of Physicists in Medicine website*. [Online] Oct 27, 2016. [Cited: Dec 12, 2016.] <https://www.aapm.org/meetings/09SS/documents/06DeWard-IonChambersInstrumentation.pdf>.
68. **H, Micheal.** Fermi National Accelerator Laboratory. *Fermi National Accelerator Laboratory website*. [Online] Nov 29, 2011. [Cited: Dec 10, 2016.] http://muon.fnal.gov/Personnel/Leveling/References/27_-_Ionization_Chambers_IV.pdf.
69. *Ion-recombination correction for different ionization chambers in high dose rate flattening-filter-free photon beams.* **Lang S, Hrbacek J, Leong A, Klock S.** 9, Zurich : Phys.Med.Biol, 2012, Vol. 57. 10.1088/0031-9155/57/9/2819.
70. *A methodological approach to reporting corrected small field relative outputs.* **Sargison GC, Charles PH, Trapp JV, Thwaites DL,** Saskoon : Elsevier, 2013, Vol. 109. 10.1016/j.radonc.2013.10.002.
71. **Inc, RD.** RD Inc Expert Service. *Radiation Products Design, Inc website*. [Online] 2016. [Cited: Sep 10, 2016.]
72. Radiation Products Design, Inc. *Radiation Products Design, Inc. website*. [Online] RD Inc . [Cited: December 22, 2016.] <http://www.rpdinc.com/ptw-31016-0016cc-pinpoint-3d-chamber--977.html>.
73. **PTW, Freiberg.** PTW Freiberg. *PTW Freiberg website*. [Online] 12 06, 2013. [Cited: 02 15, 2017.] <http://www.ptw.de/2215.html?&L=2&cId=>.
74. **American Association of Physicists in Medicine Task Group No.40.** *Comprehensive QA for Radiation Oncology*. Virginia : American Association of Physicists in Medicine, 1994. 1-56396-401-5.
75. *Detector dose response in megavoltage small photon beams. I. Theoretical concepts.* **Bouchard H, Seuntjens J, Duane S, Kamio Y, Palmans H.** 10, Teddington TW11 0LW : Med. Phys., 2015, Vol. 42. 10.1118/1.4930053.
76. *Determination of the $k_{Q_{clin}}$, $Q_{msrf_{clin}}$, f_{msr} correction factors for detectors used with an 800 MU/min CyberKnife® system equipped with fixed collimators and a study of detector response to small photon beams using a Monte Carlo method .* **Moignier C, Huet C, Makovicka L.** 7, Fontenay-aux-Roses : Med. Phys., 2014, Vol. 41. 10.1118/1.4881098.

77. **Charles M, Dennis T.** *Principles and practice of radiation therapy*. London : Elsevier Health sciences, 2015. 978-0323017480.
78. **Pannullo S, Yama C, Wernicke G.,** Intech Open Science/Open minds. *Intech Open Science/Open minds Website*. [Online] 2004 - 2016. [Cited: Jul 10, 2016.] <http://cdn.intechopen.com/pdfs/20284.pdf>.
79. **Pittsburg, University of.** Neurological Surgery (Gamma Knife). *University of Pittsburg website*. [Online] 2016. [Cited: Jul 15, 2016.] 10. <http://www.neurosurgery.pitt.edu/centers-excellence/image-guided-neurosurgery/gamma-knife>.
80. **Center, NYULangone Medical.** NYULangone Medical Center. *NYULangone Medical Center website*. [Online] 2016. [Cited: Jul 15, 2016.] http://nyulangone.org/files/NYU0596_Gamma-Knife_19.pdf.
81. **K, Christaki.** *Determination of the equivalent square small field size*. [E-mail] Vienna : International Atomic Energy Agency, 2016. RAF6044-012.
82. *Evaluation of the dose calculation accuracy for small fields defined by jaw or MLC for AAA and Acuros XB algorithms.* **Fogliata A, Lobefalo F, Reggiori G, Stravato A, Tomatis S, Scorsetti M, et al.** 10, s.l. : Med. Phys, 2016, Vol. 43. 10.1118/1.4963219.